

On Topology Inference for Networked Dynamical Systems: Principles and Performances

Yushan Li, Jianping He, Cailian Chen and Xinpeng Guan

Abstract—Topology inference for networked dynamical systems (NDSs) plays a crucial role in many areas. Knowledge of the system topology can aid in detecting anomalies, spotting trends, predicting future behavior and so on. Different from the majority of pioneering works, this paper investigates the principles and performances of topology inference from the perspective of node causality and correlation. Specifically, we advocate a comprehensive analysis framework to unveil the mutual relationship, convergence and accuracy of the proposed methods and other benchmark methods, i.e., the Granger and ordinary least square (OLS) estimators. Our method allows for unknown observation noises, both asymptotic and marginal stabilities for NDSs, while encompasses a correlation-based modification design to alleviate performance degradation in small observation scale. To explicitly demonstrate the inference performance of the estimators, we leverage the concentration measure in Gaussian space, and derive the non-asymptotic rates of the inference errors for linear time-invariant (LTI) cases. Considering when the observations are not sufficient to support the estimators, we provide an excitation-based method to infer the one-hop and multi-hop neighbors with probability guarantees. Furthermore, we point out the theoretical results can be extended to switching topologies and nonlinear dynamics cases. Extensive simulations highlight the outperformance of the proposed method.

Index Terms—Topology inference, Distributed cooperation, Networked systems, Causality and correlation modeling, Excitation-based inference.

I. INTRODUCTION

Networked dynamical systems (NDSs) are characterized by the locality of information exchange between individual nodes (described by a topology) [2], and the cooperative capability to solve a common task [3]. Inferring the interaction topology structure from observations over the system emerges in various applications in last decades, including social networks [4], brain connectivity patterns [5] and multi-robot formation [6], to name a few. As topology inference helps better understanding the systems and implementing coordinated tasks, it brings significant benefits for numerous applications of NDSs. For instance, tracing the information flow over a social network [7], group testing and identification of defective items [8], or anomaly detection in communications networks [9].

Mathematically, topology inference can be regarded as a typical inverse modeling problem. In the literature, a large body of researches has been developed to tackle the problem

The authors are with Dept. of Automation, Shanghai Jiao Tong University, Key Laboratory of System Control and Information Processing, Ministry of Education of China, and Shanghai Engineering Research Center of Intelligent Control and Management, Shanghai, Chin. E-mail address: {yushan_li, jphe, cailianchen, xpguan}@sjtu.edu.cn. The preliminary result of this paper was submitted to the 60th IEEE Conference on Decision and Control, 2021 [1].

due to their massive employments [10]. For example, [11]–[13] utilize Granger estimator to capture the causal relationships between agents. Spectral decomposition based method is also a popular tool to estimate the topology [14]–[16], which rely on the diagonalization of the sample matrices and then find the most suitable eigenvalues and eigenvectors to reconstruct the topology matrix. Kernel-based methods are widely used to identify nonlinear dynamic topology [17]–[19], where the key idea is to select appropriate kernel basis functions to approximate the nonlinear dynamics and the selection of kernels critically affects the inference performance.

Despite the prominent contributions of the pioneering works, there still remain some notable issues. First, numerous effective algorithms are designed for symmetric topology structure. The symmetry brings nice tractability in the inference procedure, e.g., in eigendecomposition for the Graph Laplacian matrix and its powers, only a group of left eigenvectors along with their corresponding eigenvalues are sufficient, avoiding large computation costs. Nevertheless, the results are hard to be generalized to account for the directed dependency between nodes, like [20], [21]. Second, most well-established techniques focus on the asymptotic performance with a large number of observation rounds or horizons (like [13], [14]), yet making it unclear how the inference error involves with the observation scale grows. Since small observation scale will give rise to poor inference results, it is also meaningful to investigate feasible techniques to improve the inference accuracy. Third, many methods are developed to interpret the latent regularity contained in the observation data by imposing edge sparsity or smoothness [22]–[24]. Although efficient, the applied technique which can be regarded as using prior knowledge, is not necessarily associated with an actual NDS structure and fails to work for general NDSs. Even for inferring the topology of NDSs, the prior knowledge about the system is assumed available beforehand, which is hard to meet in practice (e.g., the duration time of a topology in dynamic topology inference is priorly known [25]). How to relax such dependence on the prior knowledge and find effective ways to acquire it from observations are also worth consideration.

The above issues have motivated the study of this paper. We aim to present a systematic framework that well accounts for the basic principles of inferring the topology of NDSs, their mutual relationships, performances of convergence and accuracy in terms of the observation scale, along with possible revised measures to enhance the inference performance. Different from traditional system identification literatures which aim to identify the system's Markov parameters from known system input/output data (e.g., [26], [27]), the input in our

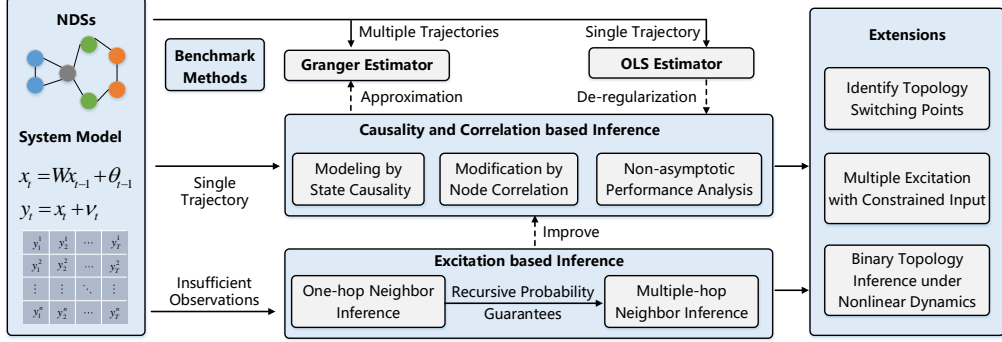


Fig. 1. The main framework of this paper.

scenario is unavailable, incurring two major challenges. On the one hand, only noisy observations over the system evolution are available, making every consecutive pair are undesirably corrupted by correlated noises. On the other hand, the observations are simultaneously influenced by the system structure, stability and process noises. The influence of noises can accumulate and incur large inference costs.

To start with, we advocate an inference method from the perspective of node causality and correlation, which account for the interaction dependence. Along this line, we reveal its close relations with popular Granger and ordinary-least-square (OLS) estimators. Then, the non-asymptotic performance of the proposed method is investigated, as well as explicit comparison with the OLS estimator and covering both marginally and asymptotically stable system dynamics. Considering the situations where the observations are not sufficient to support the estimators, the inference goal is reduced to obtain the binary connection structure contained in the topology. To practice, we propose an excitation-based method to improve the inference performance by resorting to hypothesis testing. Furthermore, we extend the estimator to identify the switching moments of dynamic topology cases, and provide a linear approximation approach to infer the binary connection structure of nonlinear system model cases. The main results are as follows.

- This work contributes to the existing body of research by revealing the principles and (non-)asymptotic performance of inferring the topology of the NDS, from the perspective of node causality and correlation. By characterizing the stability of the NDS, we demonstrate that the Granger estimator for multiple observation rounds can be approximated by a single observation round. In particular, we propose a causality-based method to effectively infer the topology from highly correlated and noisy observations, applying to both directed and undirected topologies. In addition, a correlation-based modification design is tailored for the setting on small observation scale, effectively alleviating the performance degradation by using the original causality-based method.
- By exploiting concentration of measure in Gaussian space and Chebyshev inequality, we deduce the close relations between our proposed method with the Granger and OLS estimators. Specifically, towards the Granger and proposed estimators, we prove the equivalence condi-

tions of the sample matrices in asymptotically stable system cases, and clarify the deviation growth of the matrices with the observation scale in marginally stable cases. Then, taking the OLS estimator as the benchmark of a single observation trajectory case, we derive the convergence rates of both asymptotically and marginally stable cases, i.e., $\mathcal{O}(\sqrt{\frac{1}{T}})$ and $\mathcal{O}(\sqrt{\frac{\log T}{T}})$, respectively. Concerning the inference accuracy, we enlighten in sharp contrast that the error bound in our method will converge to zero, while that of the OLS estimator converges to a bounded constant.

- Considering the situation where the observations are not sufficient to support the estimators, we develop an excitation-based approach to identify the binary connection structure in the NDS instead. Utilizing hypothesis testing, we obtain the excitation input boundary to discriminate both the one-hop and multi-hop neighbors of a node, along with the probability guarantees. Furthermore, we revise and extend the above results to more complicated topology inference scenarios, including switching topologies, general nonlinear dynamics, and bounded excitation constraints, providing a simple and efficient algorithm design. Performance study by simulation illustrates that our proposed method outperforms the OLS estimator, and verifies our theoretical results.

This paper provides deeper insights into the close relationships and the performance analysis of different inference methods. The theoretical results can serve as instructions to design the inference procedures for various observation scales, and also beckon further research to explore more advanced methods for general time-varying and nonlinear NDSs. The framework of this paper is summarized in Fig. 1.

The remainder of this paper is organized as follows. Section II presents related literatures. Section III gives basic preliminaries and describes the problem of interest. The inference methods along with their relationships are presented in Section IV. The convergence rate and accuracy of our method are analyzed in Section V. Section VI demonstrates the excitation-based inference method. Section VII discusses some extensions to more complicated cases. Simulation results are shown in Section VIII, followed by the concluding remarks and further research issues in Section IX.

II. RELATED WORK

There have been extensive researches on topology inference in the literature. Generally, it can be mainly cast into two categories: static and dynamic topology inference.

Static topology inference. In [28], [29], the authors consider the causal dynamics model and focus on learning the causal relationships by means of functional dependencies. [30] considers the network link tomography and infer the detailed topology of a measurement tree induced by multi-cast probing. Optimization algorithms are designed in [31], [32] to infer the Graph Laplacian matrix of the network from the nodal observations, by considering the stationary signals are smoothly evolving. [33] investigates the identifiability conditions for unknown dynamical networks from output second-order statistics, where the network is driven by stochastic inputs. In relation to the inference of networks from consensus dynamics, topology is reconstructed by measuring the power spectral density of the network response to input noises, and node removal strategies are designed [34], [35]. Aiming at the adaptive diffusion process of the network, the correlation methods are proposed to achieve the progressive approximation over partially observed networks [13], [36]. Note that it is difficult to accurately obtain the direct interaction between pairs of nodes using correlation methods [37]. In general, most of these works focus on specific algorithm design, and do not consider the observations can also be corrupted by independent noises, leaving it an open issue to investigate its influence and the inference performance (e.g., non-asymptotic rates and asymptotic accuracy).

Dynamic topology inference. In many applications, the observations entail a time-varying graph and static graph inference methods will fail to capture the dynamic characteristic. To account for the time-varying issue, numerous methods have been developed mainly based on the extensions of graphical Lasso-based methods [20], [38], [39] and SEM models [40]–[42]. Note that the graphical Lasso-based approaches only apply to identify undirected dynamic topologies while SEM-based methods are feasible for both undirected and directed cases. Since multiple time slots are involved, the dynamic topology inference is usually transformed into a sequential optimization problem with multiple topology variables. For example, [43] proposes a primal-dual optimization algorithm with the prior that the topology edges change smoothly. [44] addresses the inverse covariance matrix of a sequence of multivariate observations, which encodes the conditional independence between different nodes. Also, several works focus on detecting the switching points between different topologies, which is a critical premise in dynamic inference. It is usually assumed that the graphs at each instance come from specific distributions, e.g., generalized hierarchical random graph model [45], Markov random field [46].

In addition, if the dynamics of an NDS involves nonlinearities, linear models cannot accurately capture the nonlinearities despite their simplicity. Some extensions of linear models have been proposed to deal with the nonlinear dependencies, e.g., [47], [48]. However, the topology structure is assumed priorly known in these works assume, and they mainly aim to

infer the unknown edge weights. Some kernel-based methods are developed to well account for general nonlinearities, like [49]. Unfortunately, they cannot unveil the essential topology structure explicitly.

Different from the aforementioned works, this paper focus on demonstrating the basic principles of topology inference for general NDSs and exploring their (non-)asymptotic performance in terms of observation scale. With these issues settled, we further provide their extensions on switching topology and nonlinear dynamics cases.

III. PRELIMINARIES AND PROBLEM FORMULATION

A. Graph Basics and Notations

Let $\mathcal{G} = (\mathcal{V}, \mathcal{E})$ be a directed graph that models the networked system, where $\mathcal{V} = \{1, \dots, n\}$ is the finite set of nodes and $\mathcal{E} \subseteq \mathcal{V} \times \mathcal{V}$ is the set of interaction edges. An edge $(i, j) \in \mathcal{E}$ indicates that i will use information from j . The adjacency matrix $A = [a_{ij}]_{N \times N}$ of \mathcal{G} is defined such that $a_{ij} > 0$ if (i, j) exists, and $a_{ij} = 0$ otherwise. Denote $\mathcal{N}_i = \{j \in \mathcal{V} : a_{ij} > 0\}$ as the in-neighbor set of i , and $d_i = |\mathcal{N}_i|$ as its in-degree. A directed path is a sequence of nodes $\{r_1, r_2, \dots, r_j\}$ such that $(r_{i+1}, r_i) \in \mathcal{E}$, $i = 1, 2, \dots, j-1$. A directed graph has a (directed) spanning tree if there exists at least a node having a directed path to all other nodes. \mathcal{G} must have a spanning tree to guarantee that at least one node's information can reach all other nodes.

Throughout this paper, the set variable, vector and matrix are expressed in Euclid, lowercase, and uppercase font. The subscript $[.]^{ij}([.]^i)$ denotes the ij -th(i -th) entry of a matrix (vector). Let $\mathbf{0}$ be all-zero matrix in compatible dimensions, $\rho_{\min}(M)$ and $\rho_{\max}(M)$ be the smallest and largest eigenvalues of the matrix M , respectively. For square matrices M_a and M_b in the same dimensions, $M_a \succeq M_b$ ($M_a \preceq M_b$) means $M_a - M_b$ is positive-semidefinite (negative-semidefinite). Unless otherwise noted, $\|\cdot\|$ and $\|\cdot\|_F$ represent the spectral and Frobenius norm of a matrix, respectively.

B. System Model

Consider the following networked dynamical model

$$\begin{aligned} x_t &= Wx_{t-1} + \theta_{t-1}, \\ y_t &= x_t + v_t, \end{aligned} \tag{1}$$

where x_t and y_t represents the system state and corresponding observation at time t ($t = 1, 2, \dots, T$), $W \in \mathbb{R}^{n \times n}$ is the unknown interaction matrix related to the adjacent matrix A , and θ_t and v represent the process and observation noises, satisfying the following Gauss-Markov assumption.

Assumption 1. θ_t and v_t are i.i.d. Gaussian noises, subject to $N(0, \sigma_\theta^2 I)$ and $N(0, \sigma_v^2 I)$, respectively. They are also independent of $\{x_{t'}\}_{t'=0}^{t'=t}$ and $\{y_{t'}\}_{t'=0}^{t'=t}$.

Next, we present asymptotically stable matrix class \mathcal{S}_a and the (strictly) marginally stable matrix \mathcal{S}_m as follows:

$$\begin{aligned} \mathcal{S}_a &= \{Z \in \mathbb{R}^{n \times n}, \rho_{\max}(Z) < 1\}, \\ \mathcal{S}_m &= \{Z \in \mathbb{R}^{n \times n}, \rho_{\max}(Z) = 1 \text{ and the geometric} \\ &\quad \text{multiplicity of eigenvalue 1 equals to one}\}. \end{aligned} \tag{2}$$

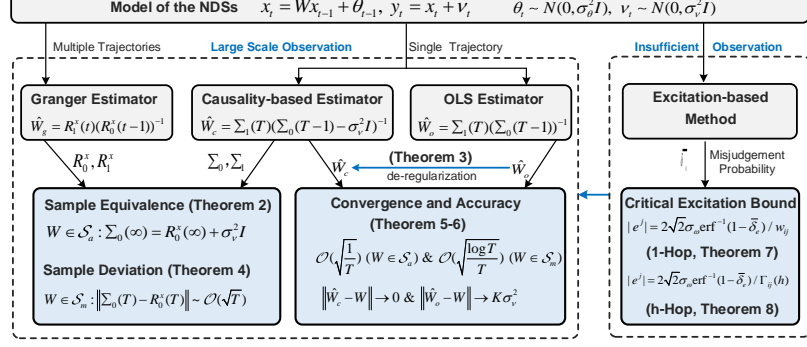


Fig. 2. Roadmap of the main theoretical results in this paper.

In terms of the setup of W , some useful and popular choices are the Laplacian and the Metropolis rules, which are defined as follows [50]. For $i \neq j$,

$$w_{ij} = \begin{cases} \gamma a_{ij} / \max\{d_i, i \in \mathcal{V}\}, & \text{by Laplacian rule,} \\ a_{ij} / \max\{d_i, d_j\}, & \text{by Metropolis rule,} \end{cases} \quad (3)$$

where the auxiliary parameter γ satisfies $0 < \gamma \leq 1$. For both rules, the self-weights are given by

$$w_{ii} = 1 - \sum_{j \neq i} w_{ij}. \quad (4)$$

Note that if W is specified by either one of the two rules, then $W \in \mathcal{S}_m$. A typical matrix in \mathcal{S}_a can be directly obtained via multiplying (3) and (4) by a factor $0 < \alpha < 1$, which is common in adaptive diffusion networks [36]. Considering different stabilities, it holds that

$$\lim_{t \rightarrow \infty} W^t = \begin{cases} \mathbf{0}, & \text{if } W \in \mathcal{S}_a \\ W^\infty, & \text{if } W \in \mathcal{S}_m, \end{cases} \quad (5)$$

where $\mathbf{0}$ represents all-zero matrix in compatible dimensions and $\|W^\infty\| < \infty$. In a recursive form, (1) is rewritten as

$$y_t = x_t + v_t = W^t x_0 + \sum_{m=1}^t W^{m-1} \theta_{t-m} + v_t. \quad (6)$$

C. Topology Inference Modeling and Problem of Interest

Given the observation sequence $\{y_t\}_{t=0}^T$ adhering to (1), the goal of this paper is to infer the unknown interaction matrix W . Mathematically, one aims to find an associated mapping

$$\phi_{\mathcal{M}} : \{y_t\}_{t=0}^T \rightarrow W. \quad (7)$$

Around the above goal, this paper is dedicated to investigating the following problems.

- From what perspectives we can design the inference methods to obtain the topology, and what are their explicit relationships among these methods.
- How is the applicability of these methods in different observation scales (e.g., single or multiple observation rounds, observation horizon, etc.), and how are their convergence and accuracy performances.
- How to infer the topology structure when the observations are not sufficient, or when the system is in more complex cases, like switching topologies and nonlinear dynamics.

To address these issues, the core challenges lie in alleviating the undesirable influence brought by highly correlated observation noises, and characterizing the inference error with limited known information. For the former one, we are able to establish an interpretable inference model borrowing the idea of node causality and correlation. For the latter, an probability analysis framework is promising to be employed by resorting to the concentration measure in Gaussian space. The main theoretical results are present in Fig. 2.

IV. TOPOLOGY INFERENCE METHODS

In this section, we first introduce two benchmark methods, the Granger and OLS estimators. Then, we propose a causality-based inference method for a single observation round setting, following by its correlation-based modification design for cases when the observation size is small. Finally, we demonstrate the close relationships among these methods.

To ease notation, we organize the state/observation/noise as

$$\begin{aligned} X_T^- &= [x_0, x_2, \dots, x_{T-1}], \quad X_T^+ = [x_1, x_2, \dots, x_T], \\ Y_T^- &= [y_0, y_2, \dots, y_{T-1}], \quad Y_T^+ = [y_1, y_2, \dots, y_T], \\ \Theta_T &= [\theta_0, \theta_1, \dots, \theta_{T-1}], \quad \Upsilon_T = [v_1, v_2, \dots, v_T]. \end{aligned} \quad (8)$$

Then, the whole evolution process is compactly written as

$$X_T^+ = W X_T^- + \Theta_T, \quad Y_T^+ = W X_T^+ + \Upsilon_T. \quad (9)$$

A. Benchmark Methods

During the running process of the NDS, the system states become highly correlated after continuous exchange of information. Therefore, the connectivity between two nodes can be revealed by the state correlation. From this perspective, the famous Pearson correlation coefficient provides a way to quantify the correlation degree, given by

$$\rho_{ij}^0 = \sum_{t=0}^T \frac{(x_t^i - \bar{x}^i)(x_t^j - \bar{x}^j)}{\rho_i^0 \rho_j^0}, \quad (10)$$

where $\rho_i^0 = \sqrt{\sum_{t=0}^T (x_t^i - \bar{x}^i)^2}$ is the sample standard deviations of $\{x_t^i\}_{t=0}^T$ and $\bar{x}^i = \sum_{t=0}^T x_t^i / T$, $\forall i \in \mathcal{V}$. The larger ρ_{ij}^0 is, the more confident one can determine that there exists an edge between node i and j .

Note that the coefficient ρ_{ij}^0 directly describes the (linear) correlation between two nodes. However, due to its symmetry,

it cannot reveal the directionality (i.e., causality) of an existing edge between two nodes. The following lemma presents a way to overcome the causality issue.

Lemma 1 (Granger causality [11], [13]). *If multiple observation round are available over the system (1), then we have*

$$R_1^x(t) = WR_0^x(t-1), \quad (11)$$

where $R_0 = \mathbb{E}[x_t x_t^\top]$ and $R_1 = \mathbb{E}[x_t x_{t-1}^\top]$ are the autocorrelation and one-lag autocorrelation matrices.

This result is straightforward since $R_1^x(t) = \mathbb{E}[x_t x_{t-1}^\top] = \mathbb{E}[(Wx_{t-1} + \theta_t)x_{t-1}^\top] = WR_0^x(t-1)$. Note that $R_0(t)$ can be explicitly represented as

$$R_0^x(t) = W^t x_0 x_0^\top (W^t)^\top + \sigma_\theta^2 \sum_{m=0}^{t-1} W^m (W^m)^\top. \quad (12)$$

According to Lemma 1, the Granger estimator is given by

- **Granger estimator:**

$$\hat{W}_g = R_1^x(t)(R_0^x(t-1))^{-1}. \quad (13)$$

Note that (13) can be interpreted as finding the coefficients $\{w_{ij}\}$ that provide the best linear prediction of x_t given the past state x_{t-1} .

Next, we present the popular OLS estimator, which is derived from the perspective of least square optimization. Then, inferring the W from $\{y_t\}_{t=0}^T$ is formulated to solve the least square problem

$$\mathbf{P}_1 : \min_W \sum_{t=1}^T \|y_t - Wy_{t-1}\|^2. \quad (14)$$

Note that the objective function of \mathbf{P}_1 can be rewritten as $\min_W \|Y_T^+ - WY_T^-\|_F^2$. Then, by finding the derivative, one obtains the optimal solution as

- **OLS estimator:**

$$\hat{W}_o = Y_T^+ (Y_T^-)^\top (Y_T^- (Y_T^-)^\top)^{-1} = \Sigma_1(T) \Sigma_0^{-1}(T). \quad (15)$$

B. Causality-based Inference Method

Although the Granger estimator presents a direct and analytic expression for inferring W , it is based on observations over multiple process rounds and the observation noises are often ignored. It cannot be directly applied in single observation round case. Nevertheless, it provides beneficial modeling ideas from the perspective of node causality. Similar with $R_0^x(t)$ and $R_1^x(t)$, we define the following sample covariance matrix and its one-lag version as

$$\Sigma_0(T) = \frac{1}{T} (Y_T^-) (Y_T^-)^\top, \quad \Sigma_1(T) = \frac{1}{T} (Y_T^+) (Y_T^-)^\top. \quad (16)$$

Before demonstrating the relationship between R_0^x/R_1^x and Σ_0/Σ_1 , we first present the asymptotic performance of Σ_0/Σ_1 .

Lemma 2 (Mutual independence between states and noises in a single round). *Given arbitrary $Z_T \in \mathbb{R}^{n \times T}$ and noise matrix $\Theta_T \in \mathbb{R}^{n \times T}$ with i.i.d. Gaussian entries. Let $|z|_m = \max\{|z_t^j| : t \in \mathbb{N}^+, j \in \mathcal{V}\}$. If $|z|_m < \infty$, then we have*

$$\Pr \left\{ \lim_{T \rightarrow \infty} \frac{1}{T} \Theta_T Z_T^\top = \mathbf{0} \right\} = 1. \quad (17)$$

Proof. The proof is provided in Appendix A. \square

Lemma 2 illustrates the independence of the sample matrix on the noise matrix in a single observation round. The result (17) also applies to linear transform $B\Theta$, where $B \in \mathbb{R}^{n \times n}$ and $\|B\| < \infty$. Since only $\{y_t\}_{t=0}^T$ are directly available, for every two adjacent observations, it follows that

$$\begin{aligned} y_t &= Wx_{t-1} + \theta_{t-1} + v_t \\ &= Wy_{t-1} - Wv_{t-1} + \theta_{t-1} + v_t \\ &= Wy_{t-1} + \omega_t, \end{aligned} \quad (18)$$

where $\omega_t = -Wv_{t-1} + \theta_{t-1} + v_t$, satisfying $N(0, \sigma_v^2 WW^\top + \sigma_v^2 I + \sigma_\theta^2 I)$, which is highly auto-correlated. Besides, ω_t is independent of all $\{x_{t'}\}_{t' < t}$ and $\{\theta_{t'}\}_{t' < t-1}$. Note that (18) only represents the quantitative relationship between adjacent observations, not a causal dynamical process. Based on the observations, we present the following theorem.

Theorem 1 (Causality in single observation round). *Given observations $\{y_t\}_{t=1}^T$, if $W \in \mathcal{S}_a$, we have*

$$\Sigma_1(\infty) = W(\Sigma_0(\infty) - \sigma_v^2 I), \quad (19)$$

where $\Sigma_1(\infty) = \lim_{T \rightarrow \infty} \Sigma_1(T)$ and $\Sigma_0(\infty) = \lim_{T \rightarrow \infty} \Sigma_0(T)$.

Proof. The proof is provided in Appendix B. \square

Different from the Granger causality in Lemma 1, Theorem 1 relaxes the dependence on multiple observation rounds, and presents the observation causality for a single round, while taking the observation noises into consideration. Then, given finite horizon T , we propose the causality-based estimator as

- **Causality-based estimator:**

$$\hat{W}_c = \Sigma_1(T)(\Sigma_0(T) - \sigma_v^2 I)^{-1}. \quad (20)$$

Remark 1. *We demonstrate that although the estimator \hat{W}_c is derived from Theorem 1 where $W \in \mathcal{S}_a$ holds, it is also applicable when $W \in \mathcal{S}_m$. In fact, Theorem 1 is directly based on the Chebyshev inequality, where the bounded state constraint precludes us from proving the convergence and accuracy of \hat{W}_c when $W \in \mathcal{S}_m$. To tackle this issue, we can resort to the concentration measure in Gaussian space. The details will be given in Section V.*

C. Correlation-based Modification Design

Like Granger estimator \hat{W}_g , the proposed causality-based estimator \hat{W}_c is a asymptotic solving manner, i.e., it will approximate the real W as $T \rightarrow \infty$. When T is small, the performance of \hat{W}_c may largely degenerate. The main cause is that directly using $\sigma_v^2 I$ to filter the influence of observation noises is not an appropriate choice, for $\sigma_v^2 I$ is a meaningful statistical characteristic in the sense of large noise samples.

Inspired by the correlation measurement (10), an alternative way to alleviate the influence of observation noises is to implement correlation coefficient calculation, which also directly represents the linear correlation between nodes. Then,

Algorithm 1 Causality and correlation based inference method

Input: Observations $\{y_t\}_{t=0}^T$, observation noise variance σ_v^2 , and the preset observation scale threshold T_p .
Output: Estimation of the topology matrix \hat{W} .

- 1: Collect all the observations into $Y_T^- = [y_0, y_2, \dots, y_{T-1}]$, $Y_T^+ = [y_1, y_2, \dots, y_T]$;
- 2: **if** $T > T_p$ **then**
- 3: Compute $\Sigma_0(T)$ and $\Sigma_1(T)$ by (16);
- 4: Estimate W by $\hat{W}_c = \Sigma_1(T)(\Sigma_0(T) - \sigma_v^2 I)^{-1}$.
- 5: **else**
- 6: For all $i \in \mathcal{V}$, compute $[\tilde{y}_t^-]^i$ and $[\tilde{y}_t^+]^i$ by (22).
- 7: Compute the sample matrices $S_0(T)$ and $S_1(T)$ by (21);
- 8: Estimate W by $\hat{W}_s = S_1(T)S_0^{-1}(T)$;
- 9: **end if**
- 10: **return** the estimation of the topology matrix \hat{W} .

we define the following correlation-based sample matrix and its one-lag version as

$$S_0(T) = \frac{1}{T} \sum_{t=0}^{T-1} \tilde{y}_t^-(\tilde{y}_t^-)^\top, \quad S_1(T) = \frac{1}{T} \sum_{t=1}^T \tilde{y}_t^+(\tilde{y}_{t-1}^-)^\top, \quad (21)$$

where the elements of \tilde{y}_t^- and \tilde{y}_t^+ are given by

$$[\tilde{y}_t^-]^i = [y_t - \frac{Y_T^- \mathbf{1}_T}{T}]^i / \rho_i^-, \quad [\tilde{y}_t^+]^i = [y_t - \frac{Y_T^+ \mathbf{1}_T}{T}]^i / \rho_i^+, \quad (22)$$

where $\mathbf{1}_T \in \mathbb{R}^T$ is the all-one vector and

$$\rho_i^- = \sqrt{\sum_{t=0}^{T-1} (y_t^i - [\frac{Y_T^- \mathbf{1}_T}{T}]^i)^2}, \quad \rho_i^+ = \sqrt{\sum_{t=1}^T (y_t^i - [\frac{Y_T^+ \mathbf{1}_T}{T}]^i)^2}.$$

Finally, the correlation-based modified causality estimator is designed as

- **Correlation-modified estimator:**

$$\hat{W}_s = S_1(T)S_0^{-1}(T). \quad (23)$$

Remark 2. The main merit of \hat{W}_s lies that it subtly takes the noise filtering and the node correlation into account at the same time by the correlation coefficient calculation. In statistics, it can be seen as a normalization operation to quantity the observations in the same measurement space.

Here we point out that correlation-based modification \hat{W}_s improves the inference performance of estimator \hat{W}_c in small observation scale, and its inference accuracy is no worse than that of \hat{W}_o (this will be verified in section VIII). Specifically, the performance improvement is significant when $W \in \mathcal{S}_a$. The reason is that the state of an asymptotically stable NDS will always converge zero, which indicates the system is mainly driven by noises regardless of the initial states. In this situation, \hat{W}_s enhances the correlation and causality between two observations.

At last, the proposed causality and correlation based inference method is summarized as Algorithm 1. Note that we introduce a preset parameter T_p to describe whether the observation scale is large, which can be set as $Kn^2 (K \in \mathbb{R}^+)$. If $T > T_p$, the estimator \hat{W}_c is adopted, or \hat{W}_s otherwise.

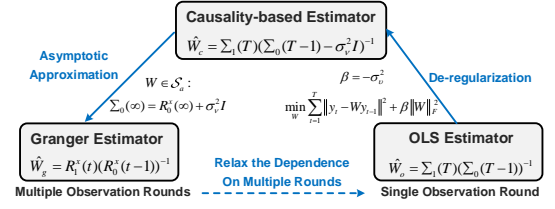


Fig. 3. An overview of the mutual relationships of \hat{W}_c , \hat{W}_g and \hat{W}_o .

D. Relationships between Different Estimators

In this part, we first demonstrate the relation between the causality-based estimator \hat{W}_c and the Granger estimator \hat{W}_g , by revealing the equivalence condition of their observation matrices in single and multiple observation rounds, respectively. The overview of the mutual relationships is shown in Fig. 3.

Theorem 2 (Equivalence condition between Σ_0 and R_0). *If $W \in \mathcal{S}_a$, when $T \rightarrow \infty$, we have*

$$\Sigma_0(\infty) = R_0^x(\infty) + \sigma_v^2 I, \quad \Sigma_1(\infty) = R_1^x(\infty) + \sigma_v^2 W. \quad (24)$$

Proof. The proof is provided in Appendix C. \square

Theorem 2 demonstrates the equivalent condition between estimators \hat{W}_g and \hat{W}_c . It reveals that the expected state covariance matrix of $T \rightarrow \infty$ is identical with the sample covariance matrix along all the single time horizon, which is an interesting result that describes the relationship between multiple and single observation rounds.

Next, consider the relationship between the causality-based estimator \hat{W}_c and OLS estimator \hat{W}_o . Note that in optimization field, it is common to use some modification on the objective function of the OLS problem to improve the solving performance, typically by adding a regularization term. Taking $\|W\|_F^2$ as the regularizer, \mathbf{P}_1 is transformed to

$$\mathbf{P}_2 : \min_W \sum_{t=1}^T \|y_t - Wy_{t-1}\|^2 + \beta \|W\|_F^2, \quad (25)$$

where β is a regularization parameter. Then, we present the following theorem.

Theorem 3 (Relationship between \hat{W}_c and \hat{W}_o). *The causality-based estimator \hat{W}_c is equivalent to solving \mathbf{P}_2 with $\beta = -\sigma_v^2$, and is a de-regularization form of \hat{W}_o .*

The proof of Theorem 3 is straightforward. Note that the objective function in \mathbf{P}_2 is equivalent to $\min_W \|Y_T^+ - WY_T^-\|_F^2 + \beta \|W\|_F^2$, whose optimal solution is

$$\hat{W} = \Sigma_1(T)(\Sigma_0(T) + \beta I)^{-1}. \quad (26)$$

Apparently, we have $\hat{W} = \hat{W}_c$ when $\beta = -\sigma_v^2$ or $\hat{W} = \hat{W}_o$ when $\beta = 0$.

Theorem 3 reveals the close relation of the proposed \hat{W}_c with \hat{W}_o . On the one hand, it provides a new interpretation for using LS methods to infer the interaction topology from the perspective of node causality. On the other hand, it illustrates the idea about how to set a reasonable regularization term and parameters for the LS problem modeling when both the input and output data are corrupted. Specifically, in the latter

case, $\beta = -\sigma_v^2$ essentially is not a typical regularization but a de-regularization form, which is quite different from normal regularization situations where $\beta > 0$.

Remark 3. *In summary, the four estimators \hat{W}_g , \hat{W}_o , \hat{W}_c and \hat{W}_s approximate W from different angles. From a pure statistical viewpoint, \hat{W}_g implements the inference over multiple rounds of observations at a single moment, while the remaining three do that over a sequence of observations in a single observation round, which is more common in practice. Specifically, \hat{W}_s is a modified version of \hat{W}_c for small horizon T , whose inference accuracy is no worse than that of \hat{W}_o .*

V. INFERENCE PERFORMANCE ANALYSIS: CONVERGENCE AND ACCURACY

In this section, we mainly analyze the inference performance of the proposed causality-based estimator \hat{W}_c in terms of convergence speed and accuracy, by comparing with \hat{W}_g and \hat{W}_o . Our analysis is based on non-asymptotic analysis of random matrices of Gaussian entries.

To begin with, we provide the supplementary results of Theorem 2 when $W \in \mathcal{S}_m$, by clarifying the non-asymptotic deviation of the observation matrices used in \hat{W}_c and \hat{W}_g .

Lemma 3 (Concentration measure in Gaussian space [51]). *Let $\Theta \in \mathbb{R}^{n \times T}$ be a matrix with independent standard normal entries. With probability at least $1 - 2 \exp(-r^2/2)$, one has*

$$\sqrt{T} - \sqrt{n} - r \leq \rho_{\min}(\Theta) \leq \rho_{\max}(\Theta) \leq \sqrt{T} + \sqrt{n} + r. \quad (27)$$

Based on Lemma 3, we demonstrate that $\Sigma_0(\infty) = R_0^x(\infty) + \sigma_v^2 I$ in Theorem 1 does not hold when $W \in \mathcal{S}_m$, but gradually deviates as T increases.

Theorem 4 (Sample matrix deviation between Σ_0 and R_0). *If $W \in \mathcal{S}_m$, the deviation norm $\|\Sigma_0(T) - R_0^x(T) - \sigma_v^2 I\|$ is at least in $\mathcal{O}(\sqrt{T})$ scale.*

Proof. The proof is provided in Appendix D. \square

Theorem 4 reveals that when $W \in \mathcal{S}_m$, the influence of the process noises will consistently accumulate over the system evolution, and one cannot use the $\Sigma_0(\infty)$ to approximate the ideal factor $R_0^x(\infty)$. However, we will demonstrate this defect does not hinder us from using the estimator to infer the topology matrix. The key question here is what is the exact influence of whether $W \in \mathcal{S}_m$ or $W \in \mathcal{S}_a$ over the inference performance. A direct intuition is that it needs extra cost to overcome the accumulated influence of process noises when $W \in \mathcal{S}_m$, compare with that when $W \in \mathcal{S}_a$. To answer this question, we let $\Sigma_T = T\Sigma_0(T-1)$ and introduce the following lemma first.

Lemma 4 (Proposition 3.1 in [52]). *Let $V \succ 0$ be a deterministic matrix and $\tilde{\Sigma}_T = \Sigma_T + V$. Given $0 < \delta < 1$ and $\{\theta_t, x_t\}_{t=1}^T$ defined as before, we have with probability $1 - \delta$*

$$\left\| \tilde{\Sigma}_T^{-\frac{1}{2}} \sum_{t=0}^{T-1} y_t v_t^\top \right\| \leq \sqrt{8n \log \left(\frac{5 \det(\tilde{\Sigma}_T V^{-1} + I)^{\frac{1}{2n}}}{\delta^{\frac{1}{n}}} \right)}. \quad (28)$$

Lemma 4 shows that there always exists an upper bound for $\left\| \tilde{\Sigma}_T^{-\frac{1}{2}} \sum_{t=0}^{T-1} y_t v_t^\top \right\|$, and the invertibility of $\tilde{\Sigma}_T$ is where most of the proof lies. In this paper, it is clear that under the Gauss-Markov assumptions, $\tilde{\Sigma}_T$ is invertible. Therefore, we can always find a Σ_{dn} and Σ_{up} such that

$$0 \prec \Sigma_{dn} \preceq X_T^{-} (X_T^{-})^\top \preceq \tilde{\Sigma}_T \preceq \Sigma_{up}. \quad (29)$$

Following Lemma 4 and (29), we present the non-asymptotic bound of \hat{W}_o , paving the way for subsequent comparisons.

Theorem 5 (Error bound by \hat{W}_o). *Given $\{y_t, \theta_t, v_t\}_{t=0}^T$ defined before, with probability at least $1 - \delta$, the following non-asymptotic bound holds,*

$$\|\hat{W}_o - W\| \leq \frac{11 \sqrt{n \log(\frac{5 \det(\Sigma_{up} \Sigma_{dn}^{-1} + I)^{\frac{1}{2n}}}{\delta^{1/n}})} + \frac{5T\sigma_v}{4\sqrt{\rho_{\min}(\Sigma_{dn})}}}{\sqrt{\rho_{\min}(\Sigma_{dn})}}. \quad (30)$$

Proof. The proof is provided in Appendix E. \square

Theorem 5 demonstrates that the non-asymptotic performance is mainly determined by $\rho_{\min}(\Sigma_{dn})$ and $\|\Sigma_{up}\|$. The non-asymptotic bound of \hat{W}_c is in the same form with that of \hat{W}_o and is omitted here. It is straightforward that if the term $\sqrt{\rho_{\min}(\Sigma_{dn})}$ grows faster than the numerator in (30) as T increases, the inference accuracy also increases. Next, we explicitly characterize the convergence and accuracy of the two estimators.

Theorem 6 (Convergence speed and accuracy of \hat{W}_o and \hat{W}_c). *With probability at least $1 - \delta$, the non-asymptotic bound of the OLS estimator \hat{W}_o satisfies*

$$\|\hat{W}_o - W\| \sim \begin{cases} \mathcal{O}(\sqrt{\frac{\log T}{T}}) + \mathcal{O}(\sigma_v^2), & \text{if } W \in \mathcal{S}_m, \\ \mathcal{O}(\frac{1}{\sqrt{T}}) + \mathcal{O}(\sigma_v^2), & \text{if } W \in \mathcal{S}_a. \end{cases} \quad (31)$$

and the non-asymptotic bound of the causality-based estimator \hat{W}_c satisfies

$$\|\hat{W}_c - W\| \sim \begin{cases} \mathcal{O}(\sqrt{\frac{\log T}{T}}), & \text{if } W \in \mathcal{S}_m, \\ \mathcal{O}(\frac{1}{\sqrt{T}}), & \text{if } W \in \mathcal{S}_a. \end{cases} \quad (32)$$

Proof. The proof is provided in Appendix F. \square

In terms of sample scale T , Theorem 6 demonstrates the convergence speed of the inference error bound by using \hat{W}_o and \hat{W}_c . Now back to the question before Lemma 4, we can conclude that the extra cost for the estimators when $W \in \mathcal{S}_m$ is longer error converging time (or larger observation sample scale), requiring $\mathcal{O}(\sqrt{\log T})$ times than that when $W \in \mathcal{S}_a$. In terms of accuracy, when $T \rightarrow \infty$, the inference error will converge to a constant by \hat{W}_o , while that of \hat{W}_c will converge to zero, which shows the latter one has better inference accuracy.

VI. EXCITATION-BASED INFERENCE METHOD

As previous sections reveal, the performance of \hat{W}_c relies on large sample scales. When the observations are extremely limited and not sufficient, it is hard to obtain a reliable W . However, we are still able to infer the logic structure of the system topology (i.e., the binary adjacent matrix). Analogous to that a stone thrown into the water will cause spreading ripples, if we apply an excitation in the node i , the influence of the excitation will quickly spread to i 's neighbor and then outer neighbors. Motivated by this, we will illustrate how to use just one-step excitation to infer the topology structure and evaluate the accuracy in this section. This method can also be applied as auxiliary measure to enhance the accuracy of the inference methods in Section IV (e.g., by treating the excitation result as a constraint in the optimization problem modeling of \hat{W}_o/\hat{W}_c).

A. Observation Model under Excitation

First, node i is called a h -hop (out)-neighbor of node j if there exists at least h edges such that

$$\prod_{l=1}^h a_{i_l i_{l+1}} = a_{i_1 i_2} a_{i_2 i_3} a_{i_3 i_4} \dots a_{i_{h-1} i_h} a_{i_h j} > 0, \quad (33)$$

where node $i_1 = i$ and $i_{h+1} = j$. Formally, the h -hop out-neighbor set can be formulated by the following recursive definition. Let $\Gamma(h) = W^h$ and $\mathcal{N}_{j,h}^e$ be the node set whose elements are connected with j within h hops, then the h -hop neighbors of j , $\mathcal{N}_{j,h}^{out}$, is given by

$$\mathcal{N}_{j,h}^{out} = \mathcal{N}_{j,h}^e \setminus \left\{ \bigcup_{l=1}^{h-1} \mathcal{N}_{j,l}^{out} \right\}. \quad (34)$$

Note that when $h = 1$, $\mathcal{N}_{j,1}^{out} = \mathcal{N}_{j,1}^e$. In the following, $\mathcal{N}_{j,1}^{out}$ is directly represented by \mathcal{N}_j^{out} , and the excitation-based method is based on the following assumption for simplicity.

Assumption 2. $W \in \mathcal{S}_a \cup \{W' : W' \in \mathcal{S}_m, W' \mathbf{1} = \mathbf{1}\}$.

Under Assumption 2 which is quite common in NDSs, when t becomes large, the difference between the elements in y_t will converge to zero in sense of expectation. In situations without excitation, two consecutive observations satisfy (18), and the observation deviation of for node i is given by

$$y_{t+1}^i - y_t^i = (W y_t)^i - y_t^i + \omega_{t+1}^i \leq \Delta y_t^{\max} + \omega_{t+1}^i, \quad (35)$$

where $\Delta y_t^{\max} = \max\{|y_t^i - y_t^j| : i, j \in \mathcal{V}\}$, $\omega_t^i \sim N(0, \sigma_\omega^2(i))$ and $\sigma_\omega^2(i)$ is given by

$$\sigma_\omega^2(i) = (1 + \sum_{j=1}^n w_{ij}^2) \sigma_v^2 + \sigma_\theta^2. \quad (36)$$

Next, let e_t^j be the excitation input on node j at time t and \tilde{y}_{t+1}^i be the observation of i under excitation. Then, the observation deviation of i under e_t^j is given by

$$\tilde{y}_{t+1}^i = \tilde{y}_{t+1}^i - y_t^i \leq \begin{cases} \Delta y_t^{\max} + w_{ij} e_t^j + \omega_t^i, & \text{if } w_{ij} > 0, \\ \Delta y_t^{\max} + \omega_t^i, & \text{if } w_{ij} = 0, \end{cases} \quad (37)$$

Note that the term $w_{ij} e_t^j$ in (37) represents the influence of the excitation input e_j over i , and all the one-hop layer neighbors

of j will have a response to the excitation in next iteration step. Then, inferring the topology by excitation is transferred to identify the one-hop neighbor set of a node j , which can be modeled as a typical binary hypothesis testing. The null hypothesis and the alternative hypothesis are respectively defined as

$$\begin{cases} H_0 : i \notin \mathcal{N}_j^{out}, \\ H_1 : i \in \mathcal{N}_j^{out}. \end{cases} \quad (38)$$

In the following parts, we will drop the subscript t in the variables if it does not cause confusion and temporarily assume $\Delta y_t^{\max} = 0$, for illustrating how to use (38) to infer the topology structure in detail.

B. One-hop Neighbor Inference

Denote $\Pr\{H_0|\tilde{y}^{i,\Delta}\}$ ($\Pr\{H_1|\tilde{y}^{i,\Delta}\}$) as the probability that H_0 (H_1) holds given the observation $\tilde{y}^{i,\Delta}$. Then, we have the following decision criterion

$$\begin{cases} \Pr\{H_1|\tilde{y}^{i,\Delta}\} \geq \Pr\{H_0|\tilde{y}^{i,\Delta}\} \Rightarrow H_1 \text{ holds,} \\ \Pr\{H_1|\tilde{y}^{i,\Delta}\} < \Pr\{H_0|\tilde{y}^{i,\Delta}\} \Rightarrow H_0 \text{ holds,} \end{cases} \quad (39)$$

which is also called the maximum posterior probability criterion. However, it is possible that (39) is misjudged in the test, for example, H_0 is true but H_1 is decided (Type I Error) or H_1 is true but H_0 is decided (Type II Error). Accordingly, let $\Pr\{D_1|H_0\}$ be the false alarm probability and $\Pr\{D_0|H_1\}$ be the missed detection probability, respectively. Therefore, the overall misjudgement probability is given by

$$\delta_e = \Pr\{D_1|H_0\} + \Pr\{D_0|H_1\}. \quad (40)$$

Suppose the inference center has no prior information about H_1 and H_0 , i.e., $\Pr(H_1) = \Pr(H_0) = 0.5$. Under (39), the inference performance by the hypothesis testing is demonstrated by the following result.

Theorem 7 (Critical excitation for one-hop neighbors). *To ensure the misjudgement probability within a threshold $\bar{\delta}_e$, the excitation e_j should satisfy*

$$|e^j| \geq \frac{2\sqrt{2}\sigma_\omega(i)}{w_{ij}} \text{erf}^{-1}(1 - \bar{\delta}_e), \quad (41)$$

where the Gaussian error $\text{erf}(z) = \frac{2}{\sqrt{\pi}} \int_0^z \exp(-r^2) dr$ and $\text{erf}^{-1}(\cdot)$ is the reverse mapping of $\text{erf}(z)$.

Proof. The proof is provided in Appendix G. \square

Theorem 7 gives the lower magnitude bound of the excitation input to guarantee the specified misjudgment probability in a single time. Given the excitation input e^j satisfying (41), one has with probability at least $(1 - \bar{\delta}_e)$ to accurately discriminate whether $i \in \mathcal{N}_j^{out}$. Note that the interaction weight w_{ij} is not priorly known in reality, thus the decision threshold in theory, $\frac{w_{ij}e^j}{2}$, is unavailable. However, we can enable the hypothesis test by specifying the least interaction weight that one wishes to discriminate between two nodes.

To practice, since $\|W\|_F \leq \sqrt{n} \|W\| \leq \sqrt{n}$, thus we have $\sum_{j=1}^n w_{ij}^2 \leq n$ and

$$\sigma_\omega^2(i) \leq (1 + n) \sigma_v^2 + \sigma_\theta^2 = \bar{\sigma}_\omega^2. \quad (42)$$

Algorithm 2 Excitation-based inference method

Input: Observations y_t , target excited node j , desired lower bound of interaction weight \underline{w} , upper bound $\bar{\sigma}_\omega$, and tolerant error probability $\bar{\delta}_e$.

Output: Estimation of the one-hop out-neighbor of j , $\hat{\mathcal{N}}_j^{out}$.

- 1: Initialize $\hat{\mathcal{N}}_j^{out} = \emptyset$.
- 2: Calculate the critical excitation $e^j = \frac{2\sqrt{2}\bar{\sigma}_\omega}{\underline{w}} \operatorname{erf}^{-1}(1 - \bar{\delta}_e)$.
- 3: Excite node j with e^j and obtain the observation y_{t+1} .
- 4: Compute $\Delta y_t^{\max} = \max\{|y_t^i - y_t^j| : i, j \in \mathcal{V}\}$.
- 5: **for** $i \in \mathcal{V}$ **do**
- 6: Compute the observation deviation $\tilde{y}_{t+1}^{i,\Delta} = y_{t+1}^i - y_t^i$.
- 7: **if** $|\tilde{y}_{t+1}^{i,\Delta}| > \Delta y_t^{\max} + \frac{\underline{w}e^j}{2}$ **then**
- 8: $\hat{\mathcal{N}}_j^{out} = \hat{\mathcal{N}}_j^{out} \cup \{i\}$.
- 9: **end if**
- 10: **end for**
- 11: **return** The one-hop neighbor set estimation $\hat{\mathcal{N}}_j^{out}$.

Specifically, if W is row-stochastic, then the upper bound $\bar{\sigma}_\omega^2$ can be further reduced to $2\sigma_v^2 + \sigma_\theta^2$. Next, suppose that one aims to judge whether $i \in \mathcal{N}_j^{out}$ such that $w_{ij} > \underline{w}_{ij}$, where w_{ij} is the specified weight threshold. Given the desired error probability bound $\bar{\delta}_e$ and the excitation input e^j such that $e^j = \frac{2\sqrt{2}\bar{\sigma}_\omega}{\underline{w}} \operatorname{erf}^{-1}(1 - \bar{\delta}_e)$, then with probability at $1 - \bar{\delta}_e$ one can discriminate whether $i \in \mathcal{N}_j^{out}$ by

$$\begin{cases} i \in \mathcal{N}_j^{out}, & \text{if } |\tilde{y}_{t+1}^{i,\Delta}| \geq \Delta y_t^{\max} + \frac{w_{ij}|e^j|}{2} \\ i \notin \mathcal{N}_j^{out}, & \text{else,} \end{cases} \quad (43)$$

where the parameters in (43) are all computable or known. Applying (43) to all other node and one can obtain an estimated set of \mathcal{N}_j^{out} . The whole procedures are summarized in Algorithm 2.

Remark 4. The key point of using the excitation-based method lies in that it requires certain prior knowledge about $|(W y_t)^i - y_t^i|$ or the evolution characteristic of y_t . In this paper, we utilize Assumption 2 to bound $|(W y_t)^i - y_t^i|$ for simplicity. Many other ways are also applicable and are not the interest of this paper. Besides, if a lower bound estimator of an edge weight w_{ij} is available, the inference accuracy can be further improved.

A direct result from Theorem 7 is $\lim_{|e^j| \rightarrow \infty} \delta_e = 0$, which corresponds to the common intuition. As long as the excitation input is large enough, the one-hop neighbors of j can always be inferred. Under this situation, it is also very likely that the two-hop (even more) out-neighbors of the excited node can be also identified by just single excitation.

C. Multi-hop Neighbor Inference

In this part, we will demonstrate how to identify multi-hop out-neighbors of a node by single excitation. Similar with the

hypothesis (38), we first define the following hypothesis that tests whether $i \in \mathcal{N}_{j,h}^e$, i.e.,

$$\begin{cases} H_0(h) : i \notin \mathcal{N}_{j,h}^e, \\ H_1(h) : i \in \mathcal{N}_{j,h}^e. \end{cases} \quad (44)$$

Lemma 5 (Critical excitation for neighbors within h hops). *Under hypothesis test (44), to ensure the misjudgement probability for all the neighbor within h -hop is lower than $\bar{\delta}_e$, the excitation e_j should satisfy*

$$|e^j| \geq \frac{2\sqrt{2}\bar{\sigma}_\omega}{\Gamma_{ij}(h)} \operatorname{erf}^{-1}(1 - \bar{\delta}_e), \quad (45)$$

Proof. Directly focusing on the h -step node response after the excitation input is injected on j , $\Gamma(h)$ becomes the equivalent topology that corresponds to the h -step process. Based on Theorem 7, when $|e^j| \geq \frac{2\sqrt{2}\bar{\sigma}_\omega}{\Gamma_{ij}} \operatorname{erf}^{-1}(1 - \bar{\delta}_e)$ ensures the misjudgement probability is no more than $(1 - \bar{\delta}_e)$, which completes the proof. \square

Note that Lemma (5) only illustrates how to reduce the misjudgement probability of $i \in \mathcal{N}_{j,h}^e$, and does not provide information about whether $i \in \mathcal{N}_{j,h}^{out}$. A key insight is that if i is decided not in $\mathcal{N}_{j,h-1}^e$ but in $\mathcal{N}_{j,h}^e$, then it is very likely that $i \in \mathcal{N}_{j,h}^{out}$ is true. Starting from this point, we utilize a single-time excitation input and do h -rounds tests to achieve the inference goal. Two auxiliary functions are defined as

$$F_0(z, e^j) = \int_{\frac{ze^j}{2}}^{+\infty} \frac{1}{\sqrt{2\pi\sigma_\omega^2}} \exp\left(-\frac{r^2}{2\sigma_\omega^2}\right) dr, \quad (46)$$

$$F_1(z, e^j) = \int_{\frac{ze^j}{2}}^{+\infty} \frac{1}{\sqrt{2\pi\sigma_\omega^2}} \exp\left(-\frac{(r - ze^j)^2}{2\sigma_\omega^2}\right) dr, \quad (47)$$

where $z \in [0, 1]$. Based on $F_0(z)$ and $F_1(z)$, the inference probability of multi-hop out-neighbors is presented as follows.

Theorem 8 (Lower probability bound of neighbor inference). *Given the maximum false alarm probability α , implement the test (44) from 1-hop to h -hop and the single-time excitation input $e^j \geq e_m^j = \frac{2\sqrt{2}\bar{\sigma}_\omega \operatorname{erf}^{-1}(1-2\alpha)}{\Gamma_{ij}^{\min}}$, we have*

$$\Pr\{i \in \mathcal{N}_{j,h}^{out}\} \geq F_1(\Gamma_{ij}^{\min}, e_m^j)(2 - \alpha - F_1(\Gamma_{ij}^{\max}, e_m^j)), \quad (48)$$

where Γ_{ij}^{\min} and Γ_{ij}^{\max} are given by

$$\begin{cases} \Gamma_{ij}^{\min} = \min\{\Gamma_{ij}(l), l = 1, \dots, h\}, \\ \Gamma_{ij}^{\max} = \max\{\Gamma_{ij}(l), l = 1, \dots, h\}. \end{cases} \quad (49)$$

Proof. The proof is provided in Appendix H. \square

Theorem 8 provides the lower probability bounds for $\Pr\{i \in \mathcal{N}_{j,h}^{out}\}$ given the maximum false alarm probability α of the test (44) in each round. A notable characteristic of the bounds is that with just a single time excitation input, they can be calculated recursively. The higher the hop number is, the lower the probability bound is. The practical application of this test is similar to (43) and omitted here.

As a summary of the theoretical analysis in aforementioned sections, we present the performance comparisons of our proposed causality-based and excitation based methods, and other typical algorithms in Table I.

TABLE I
COMPARISONS OF THE PROPOSED METHOD WITH OTHER REPRESENTATIVE ALGORITHMS

Method	Topology Structure		System Stability		Noise Consideration		Convergence Speed	Asymptotic Error
	Undirected	Directed	Asymptotical	Marginal	Process	Observation		
Granger estimator in [13]	✓		✓		✓		$\mathcal{O}(\sqrt{\frac{1}{L}})^1$	constant
Spectral method in [21]	✓				✓		$\mathcal{O}(e^{-L})^2$	zero (noise-free)
OLS estimator		✓	✓	✓	✓		up to $\mathcal{O}(\sqrt{\frac{\log T}{T}})^3$	constant
Our method	✓		✓	✓	✓	✓	up to $\mathcal{O}(\sqrt{\frac{\log T}{T}})$	zero
Excitation-based method	✓		✓	✓	✓	✓	at least $\mathcal{O}(\text{erf}(e_j))^4$	zero

¹ L here refers to the number of multiple trajectories. ² In [21] the authors implement multiple times of observation over the system, with the same initial state while ending at different moments, and no noise terms are involved. ³ T here refers to the number of the observation horizon in single trajectory.

⁴ We remark the convergence here refers to the probability that the positive hypothesis is right, corresponding to $1 - \delta_e \xrightarrow{|e^j| \rightarrow \infty} 1$.

VII. EXTENDED DISCUSSIONS

In this section, we provide some extended the results in Section V and VI to more complex cases of NDSs.

A. Identification of Switching Topologies

In many cases, the topology structure dynamically changes with time due to factors, e.g., the communication link between two nodes lost. It is a quite challenging issue to infer the internal topologies series from the observations. Most existing works generally assume that the switching moment between two adjacent topologies is priorly known, which is impractical in many situations. Based on the following assumption, we propose a switching-identification method to illustrate how to find the switching moments and evaluate the performance.

Assumption 3. *The topology does not quickly switch and each topology should maintain at least for a certain slot (e.g., $n+1$ moments). All the possible topologies must contain at least one spanning tree.*

Corollary 1 (Error bound of state prediction). *Given y_t , suppose we have an estimate \hat{W} of W and predict y_{t+1} by $\hat{y}_{t+1} = \hat{W}y_t$, then we have*

$$\mathbb{E}\{\|\hat{y}_{t+1} - y_{t+1}\|^2\} \leq \|\hat{W} - W\|^2\|y_t\|^2 + 2\sigma_v^2 + \sigma_\theta^2. \quad (50)$$

Proof. Following from the observation relationship (18), the key point is that given $y_t, v_t, \theta_t, v_{t+1}$ are all independent of each other and their prediction errors are uncorrelated. Then, given $\hat{y}_{t+1} = \hat{W}y_t$, one has

$$\hat{y}_{t+1} - y_{t+1} = (\hat{W} - W)y_t + Wv_t - v_{t+1} - \theta_t. \quad (51)$$

Then, it follows from (51) that

$$\begin{aligned} & \mathbb{E}\{(\hat{y}_{t+1} - y_{t+1})(\hat{y}_{t+1} - y_{t+1})^\top\} \\ &= (\hat{W} - W)y_t y_t^\top (\hat{W} - W)^\top + \sigma_v^2 (W W^\top - I) + \sigma_\theta^2 I. \end{aligned} \quad (52)$$

Hence, by utilizing $\|W\| \leq 1$ one has $\mathbb{E}\{\|\hat{y}_{t+1} - y_{t+1}\|^2\} = \|\hat{W} - W\|^2\|y_t\|^2 + 2\sigma_v^2 + \sigma_\theta^2$. The proof is completed. \square

Corollary 1 gives the observation prediction error bound in sense of expectation, potentially providing a beneficial tool to

identify whether the system topology has changed. In practice, if the $\|\hat{y}_{t+1} - y_{t+1}\|^2$ exceeds the bound given by (50), then with high probability the original topology has switched. Consequently, the switching moment is also found, which lays the foundation to infer the topologies in different time slots. Note that if the topology matrix is row-stochastic, then the upper bound is further reduced to $\|\hat{W} - W\|_F^2\|y_t\|^2 + 2\sigma_v^2 + \sigma_\theta^2$.

Remark 5. *Using (50) only plays a sufficient role to identify the topology switches. In fact, it is totally possible that even a topology changes, the resulting state is still the same as the one by the original topology. Therefore, we claim that there is no necessary condition for an identifiable topology switching from the perspective of the state deviation.*

B. Inference by Multiple Excitations

Theorem 7 and 8 illustrate the conditions and performances of using just one-time excitation, however, there are also situations where a large excitation input is not allowed in the network dynamics, making the methods not directly available. To overcome this deficiency, multi-excitation is a promising alternative to achieve the inference goal. In this part, we will briefly show how to address the issue.

Suppose node j is excited m times with the same excitation input e^j , the inference center obtains the average observation deviation of m rounds by $\hat{y}_m^{i,\Delta} = \frac{1}{m} \sum_{l=1}^m y^{i,\Delta}(l)$.

Corollary 2 (Upper bound of the misjudgement probability under multiple excitations). *Given excitation input $e^j > 0$ and implement m times of excitations, the misjudgement probability satisfies*

$$\delta_e(m) \leq 2 \int_{\frac{q_0 e^j}{2}}^{+\infty} \frac{1}{\sqrt{2\pi}\sigma/\sqrt{m}} \exp\left(-\frac{z^2}{2\sigma^2/m}\right) dz, \quad (53)$$

where $q_0 = \min\{w_{ij} : j \in \mathcal{V}\}$.

Proof. Based on the independent identically distributed characteristic of $y^{i,\Delta}(l)$, $y^{i,\Delta}(l)$ is subject to $N(0, \frac{\sigma^2}{m})$. Then, the

misjudgement probability is calculated by

$$\begin{aligned}
\delta_e(m) &= \Pr\{D_1|H_0\} + \Pr\{D_0|H_1\} \\
&= \int_{\frac{w_{ij}e^j}{2}}^{+\infty} \frac{1}{\sqrt{2\pi}\sigma_\omega/\sqrt{m}} \exp\left(-\frac{z^2}{2\sigma_\omega^2/m}\right) dz \\
&\quad + \int_{-\infty}^{\frac{w_{ij}e^j}{2}} \frac{1}{\sqrt{2\pi}\sigma_\omega/\sqrt{m}} \exp\left(-\frac{(y - w_{ij}e^j)^2}{2\sigma_\omega^2/m}\right) dz \\
&= 2 \int_{\frac{w_{ij}e^j}{2}}^{+\infty} \frac{1}{\sqrt{2\pi}\sigma_\omega/\sqrt{m}} \exp\left(-\frac{z^2}{2\sigma_\omega^2/m}\right) dz \\
&\leq 2 \int_{\frac{q_0e^j}{2}}^{+\infty} \frac{1}{\sqrt{2\pi}\sigma_\omega/\sqrt{m}} \exp\left(-\frac{z^2}{2\sigma_\omega^2/m}\right) dz, \quad (54)
\end{aligned}$$

which completes the proof. \square

It is easy to see from Corollary 2 that, as m grows the variance σ_ω^2/m decrease and so does $\delta_e(m)$. Therefore, it follows that

$$\lim_{m \rightarrow \infty} \delta_e(m) = 0. \quad (55)$$

Corollary 2 illustrates that even when the magnitude of the excitation input is constrained, the misjudgment probability can be significantly reduced by increasing the excitation times. Due to w_{ij} is not priorly known, we can relax the decision threshold as in (43). Given the maximum available excitation input e_{\max}^j and specified weight threshold \underline{w}_{ij} , one has with probability at least $1 - \bar{\delta}_{e,m}$ to discriminate whether $i \in \mathcal{N}_j^{\text{out}}$ by the following multiple excitation testing

$$\begin{cases} i \in \mathcal{N}_j^{\text{out}}, & \text{if } |\tilde{y}_m^{i,\Delta}| \geq \frac{\sum_{l=1}^m \Delta y^{\max}(l)}{m} + \frac{w_{ij}e_{\max}^j}{2}, \\ i \notin \mathcal{N}_j^{\text{out}}, & \text{else,} \end{cases} \quad (56)$$

where $\bar{\delta}_{e,m} = 2 \int_{\frac{\underline{w}_{ij}e_{\max}^j}{2}}^{+\infty} \frac{1}{\sqrt{2\pi}\sigma_\omega/\sqrt{m}} \exp\left(-\frac{z^2}{2\sigma_\omega^2/m}\right) dz$. A minor drawback of this method is that if the weight between two nodes is small and the excitation time is also limited, an existing edge may be regarded as not existing.

C. Nonlinear Cases

The nonlinearities of the NDS model mainly come from two aspects. First, the magnitude of the system state cannot be unbounded, thus the input torque is bounded [53]. Second, the edge weight in the topology matrix is not necessarily static, and it can be highly dependent on the state difference of its associated two nodes [54]. Mathematically, the two kinds of nonlinearities can be uniformly formulated by

$$x_{t+1}^i = x_t^i + \sum_{j=1}^n \varphi_{ij}(x_t^j - x_t^i), \quad (57)$$

where $\varphi_{ij}(z)$ is a continuous and strictly-bounded function, and $\varphi_{ij}(z) = 0$ if $a_{ij} = 0$ or $z = 0$. As for the conditions of φ_{ij} to guarantee the convergence and stability of the NDS, the readers are referred to [54]. Note that it is difficult to obtain the actual input form of each agent and find the internal edge weight, however, their internal adjacent structure is unchanged, which is also critical knowledge about the NDS.

Next, we will illustrate how to use our proposed revised casualty-based estimator to infer the adjacent structure. The

Algorithm 3 Infer the topology structure of nonlinear cases

Input: Observations $\{y_t\}_{t=0}^T$, and node set \mathcal{V} .
Output: Binary adjacent matrix estimator $\hat{A} = [\hat{a}_{ij}]_{i=1:n}^{j=1:n}$.

- 1: Calculate the total regression time $T' = T - n + 1$.
- 2: **for** $l \leftarrow 1$ **to** T' **do**
- 3: **for** $i \in \mathcal{V}$ **do**
- 4: $\rho_i^-(l) = \sqrt{\sum_{t=l}^{l+n-1} (y_t^i - [\frac{Y_{l:n-1}^- \mathbf{1}_n}{n}]^i)^2}$,
- 5: $\rho_i^+(l) = \sqrt{\sum_{t=l+1}^{l+n} (y_t^i - [\frac{Y_{l+1:n}^- \mathbf{1}_n}{n}]^i)^2}$.
- 6: $[\tilde{y}_t^-]^i = [y_t - Y_{l:l+n-1}^- \mathbf{1}_n/n]^i / \rho_i^-$,
- 7: $[\tilde{y}_t^+]^i = [y_t - Y_{l+1:l+n}^- \mathbf{1}_n/n]^i / \rho_i^+$.
- 8: **end for**
- 9: $\tilde{W}(l) = \arg \min_{W(l)} \frac{1}{n} \sum_{t=l}^{l+n-1} \|\tilde{y}_{t+1} - W(l)\tilde{y}_t\|_2^2$.
- 10: Adopt k -means method to $\tilde{W}(l)$ and obtain its corresponding binary adjacent matrix $\tilde{A}(l) = [\tilde{a}_{ij}(l)]_{i=1:n}^{j=1:n}$.
- 11: **end for**
- 12: **for** $i, j \in \mathcal{V}$ **do**
- 13: $\mathcal{A}_0^{ij} = \{\tilde{a}_{ij}(l) = 0 : l = 1, \dots, T'\}$,
- 14: $\mathcal{A}_1^{ij} = \{\tilde{a}_{ij}(l) > 0 : l = 1, \dots, T'\}$.
- 15: $\hat{a}_{ij} = 1$ if $|\mathcal{A}_1^{ij}| > |\mathcal{A}_0^{ij}|$ or $\hat{a}_{ij} = 0$ otherwise.
- 16: **end for**

key idea is as follows. First, we adopt linearization over a local time horizon sequentially and calculate the topology matrix by estimator (23). Since W contains n^2 element, at least $n + 1$ groups of consecutive observations y are needed to obtain a least square solution of W (suppose $y_{t+1} = Wy_t$). Therefore, we set the local time horizon as $n + 1$. Then, all the estimated topology matrices are integrated to discriminate whether an edge between two nodes exists in sense of statistics. Specifically, a clustering procedure (e.g., k -means cluster method) is adopted to automatically classify the regressed weights into connected and disconnected ones. To strengthen the classification accuracy, a voting rule is proposed to determine the connectivity of every pair of nodes. The whole procedures are summarized as Algorithm 3.

It is remarkable that since $\varphi_{ij}(x^j - x^i) \neq 0$ if $a_{ij} \neq 0$ and $x^j - x^i \neq 0$, then the excitation-based method in Section VI is also available to identify the topology structure in nonlinear cases, especially when the observations are limited. The process is likewise to that of the linear case and is omitted here due to the space limit.

VIII. NUMERICAL EXPERIMENTS

In this section, we present extensive numerical experiments to demonstrate the effectiveness of our proposed methods, with reference to the classical Granger estimator and ordinary least estimator. First, we display the basic setup of the whole experiment. Then, we conduct groups of experiments under different conditions, including the system stability, observation scale and noise variance. Detailed analysis is also provided to demonstrate the performance of our method.

A. Simulation Setup

The most critical components are the adjacent matrix A and the interaction matrix W . We randomly generate a directed

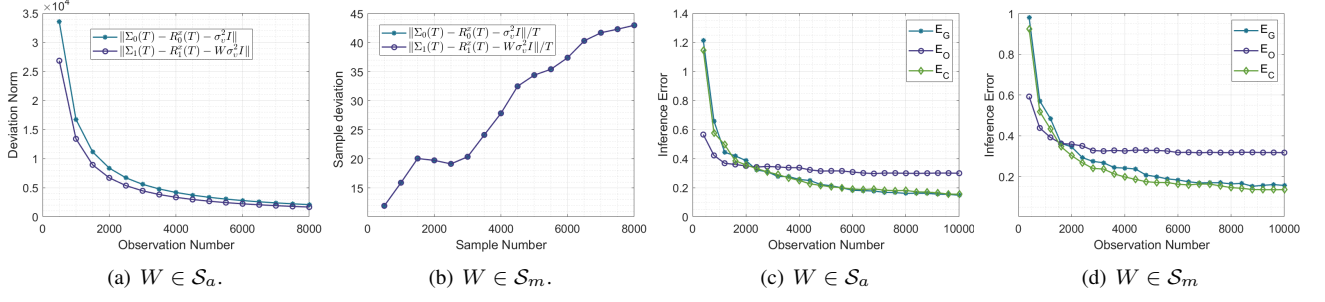


Fig. 4. The sample matrix deviation and inference performance of E_G utilizing multiple observation trajectories and E_C utilizing single observation trajectory. The same topology structure and initial system state are set for two groups of experiments. (a)(b): Sample matrix deviation. (c)(d): Inference performance.

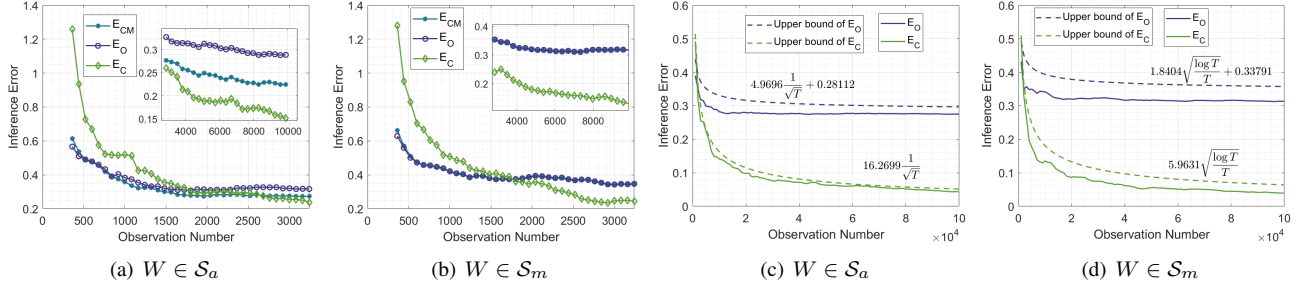


Fig. 5. Performance comparison of E_O , E_C and E_{CM} utilizing single observation trajectory. The same topology structure and initial system state are set for two kinds of experiments. (a)(b): Results in small observation scale. (c)(d): Non-asymptotic rates as T increases.

topology structure with $|\mathcal{V}| = 20$, and the weight of W is designed by the Laplacian rule. Both $W \in \mathcal{S}_a$ and $W \in \mathcal{S}_m$ are considered. For generality, the initial states of all agents are randomly selected from the interval $[400, 600]$, and the variance of the process and observation noise satisfy $\sigma_\theta^2 = 1$ and $\sigma_v^2 = 1$. To evaluate the inference accuracy, we use the following index as

$$error = \|\hat{W} - W\|. \quad (58)$$

For simple expression, hereafter we denote the Granger estimator (13), the OLS estimator (15), the proposed causality-based method (20) and the correlation-based modification method (23) by E_G , E_O , E_C and E_{CM} , respectively.

B. Results and Analysis

Let us begin with examining the sample matrix deviation in E_G and E_C , i.e., conclusions in Theorem 2 and 4. The results are reported in Fig. 4(a) and Fig. 4(b). When $W \in \mathcal{S}_a$, the sample matrix $R_0^x(T)$ from multiple observation trajectories can be approximated by the sample matrix $\Sigma_0(T)$ from single observation trajectory as $T \rightarrow \infty$. When $W \in \mathcal{S}_m$, the deviation norm between $R_0^x(T)$ and $\Sigma_0(T)$ goes to infinity as $T \rightarrow \infty$ as shown in Fig. 4(b), and this is because the influence of the process noise will remain as the system evolves. Then, we directly present the inference errors of the methods in terms of sample size, covering both marginal and asymptotic cases. By joint inspection of Fig. 4(c) and Fig. 4(d), the accuracy magnitudes of E_G and E_C are very close, which verifies the conclusion of Theorem 1 that the inference result from a single observation round becomes equivalent with that from multiple

observation rounds when $T \rightarrow \infty$. Besides, it is found that E_C behaves worse than E_O when in small observation scale, but outperforms E_O asymptotically, while the accuracy of E_C remains stable as the data size increase. The main reason is that the statistical characteristic of observation noises will matter a lot when the observation scale is large, which is not taken into account by the OLS method.

Next, the inference performance of E_O , E_C and E_{CM} are evaluated under the same single observation round, as demonstrated in Fig. 5. For a asymptotic stable NDS, E_{CM} outperforms E_O asymptotically but is still worse than E_C , as illustrated in Fig. 5(a). For a marginal stable NDS, E_{CM} has almost the same inference performance as E_O , shown in Fig. 5(b). We note that E_C applies to cases with a large observation scale, while E_{CM} applies to other situations with no worse performance than E_O . In Fig. 5(c) and Fig. 5(d), the analysis of the non-asymptotic inference errors in Theorem 6 is verified. The upper bounds of the inference errors of two estimators are drawn in the figures, providing explicit expressions in terms of the observation scale T . From the inset plots, we can appreciate that the proposed E_C exhibits better performance than E_O . Remarkably, the inference error of E_C converges to zero while that of E_O converges to constant, as T increases.

Now we move on to verify the performance excitation-based method, as shown in Fig. 6. Specifically, we excite a target node j and wish to find its one-hop out-neighbor i subject to $w_{ij} \geq 0.4$ in case of $W \in \mathcal{S}_a$ and $w_{ij} \geq 0.5$ in case of $W \in \mathcal{S}_m$. Given the lower probability bound $\bar{\delta}_e$, the critical excitation input is calculated by $|e^j| = \frac{2\sqrt{2}\sigma_{\omega(i)}}{w_{ij}} \text{erf}^{-1}(1 - \bar{\delta}_e)$. Then, we use the input to conduct the test 1000 times and

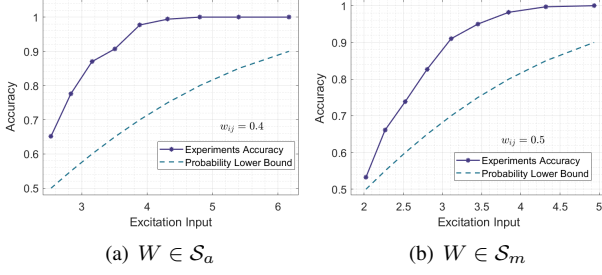


Fig. 6. Example of inferring single-hop neighbors of a node using excitation-based inference results. The accuracy is obtained by implementing the test 1000 times and computing the ratio of positive results.

computing the ratio of positive results. As one expects, larger excitation input ensures higher accuracy of the decision results, and given the same level probability lower bound, smaller topology weight requires larger excitation input magnitude (comparing Fig. 6(a) with Fig. 6(b)). We note that the dashed lines are lower bounds of the accuracy in theory, thus it makes sense that the actual accuracy in experiments is higher than that bound. The multi-hop neighbor inference and multiple excitation cases are likewise and are omitted here.

Finally, we focus on the evolution of Algorithm 3 in nonlinear dynamics cases, namely, inferring the binary topology structure in the NDS. To this end, we adopt two representative cases of nonlinear model $x_{t+1}^i = x_t^i + \sum_{j=1}^n \varphi_{ij}(x_t^j - x_t^i) + \theta_t^i$, where φ_{ij} is given by

$$\text{Case 1 : } \varphi_{ij} = \frac{\text{sign}(a_{ij})|x_t^j - x_t^i|(x_t^j - x_t^i)}{1 + \sum_{j \in \mathcal{N}_i} (x_t^j - x_t^i)^2}, \quad (59)$$

$$\text{Case 2 : } \varphi_{ij} = a_{ij}(x_t^j - x_t^i) \left(\frac{2}{1 + \exp\{-(x_t^j - x_t^i)\}} - 1 \right).$$

According to the sufficient conditions in [54], both the two systems will reach stable states when noise-free. We repeat the experiments under different process noise level with segment number in Algorithm 3 increases, where σ_θ is set as 0.02, 0.2, 0.5 and 1, respectively. Here to evaluate the performance of Algorithm 3, we adopt the structure error index, given by

$$\text{error}_s = \|\text{abs}(\hat{A} - A)\|_0 / N^2, \quad (60)$$

where $\text{abs}(\cdot)$ means obtaining the absolute value of each entry in the matrix variable, and $\|\cdot\|_0$ represents the number of non-zero entries of matrix. As we can see, the accuracy generally grows with the segment number at first and remains stable when the number is large. Perhaps unexpectedly, given the same segment number, the inference accuracy trend in the former case does exhibit the trend in the latter one, where the accuracy increases with σ_θ . However, we remark that this behavior is determined by the intrinsic characteristic of nonlinear dynamics, and when the noise variance exceeds a certain value, the accuracy will not change a lot.

IX. CONCLUSIONS

In this paper, we investigated the principles and performances of inferring the topology of NDSs, from the perspective of node causality and correlation. First, we propose

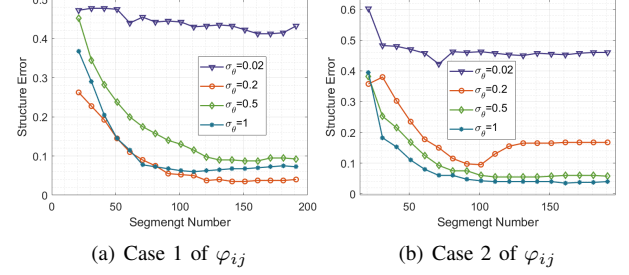


Fig. 7. Examples of inferring the topology structures of nonlinear dynamics $x_{t+1}^i = x_t^i + \sum_{j=1}^n \varphi_{ij}(x_t^j - x_t^i) + \theta_t^i$.

a causality-based estimator that allows for the presence of unknown observation noises, along with its correlation-based modification design to alleviate performance degradation in a small observation scale. By relating the proposed estimator for a single observation round with the Granger estimator for multiple rounds, we prove their equivalence when the NDS is asymptotically stable, and demonstrate the incremental characteristic of their sample matrices deviation in marginally stable cases. Then, we rigorously analyzed the convergence rate and accuracy of the proposed estimator by utilizing concentration measure, demonstrating that our method has superior inference performance to the OLS estimator. Besides, for cases where the observations are not sufficient to support the above estimators, an excitation-based method was designed to infer the binary topology structure in the NDSs by leveraging hypothesis testing. Finally, some extensions on switching topologies, nonlinear dynamics and multi-step excitation scenarios were discussed. Performance study by simulations verified our performance analysis.

The study of this paper provides meaningful insights into the topology inference problem, and paves the way for several interesting avenues of future research, including i) investigating a richer class of NDS models, including non-stochastic input and generative switching topologies cases; ii) developing more novel nonlinear inference algorithms (e.g., online, distributedly) with certain node causality and correlation as priors; iii) analyzing the performance of the topology inference methods for NDSs under more complicated dynamic settings; and iv) using the inference methods to topology-related applications, like anomaly detection and state prediction in NDSs.

APPENDIX

A. Proof of Lemma 2

Proof. The proof is conducted in element-wise analysis. To ease notation, we denote $\Xi(T) = \frac{1}{T} \Theta_T Z_T^\top = \sum_{t=1}^T \theta_{t-1} z_{t-1}^\top$, and the element $\Xi_{ij}(T) = \frac{1}{T} [\Theta_T Z_T^\top]^{ij}$ is calculated by

$$\Xi_{ij}(T) = \frac{1}{T} \sum_{t=1}^T \theta_{t-1}^i z_{t-1}^j. \quad (61)$$

Since $\theta_t \sim \mathcal{N}(0, \sigma^2)$, it follows that

$$\mathbb{E}[\Xi_{ij}(T)] = \frac{1}{T} \sum_{t=1}^T \mathbb{E}[\theta_{t-1}^i] z_{t-1}^j = 0, \quad (62)$$

$$\mathbb{D}[\Xi_{ij}(T)] = \sum_{t=1}^T \left(\frac{z_{t-1}^j}{T} \right)^2 \sigma^2 \leq \frac{(|z|_{\max}^j)^2 \sigma^2}{T}, \quad (63)$$

where $|z|_{\max}^j = \max\{|z_t^j|, t = 0, 1, \dots, T-1\}$. By the famous Chebyshev inequality, given arbitrary $\epsilon > 0$, we have

$$\Pr\{|\Xi_{ij}(T)| < \epsilon\} \geq 1 - \frac{\mathbb{D}[\Xi_{ij}(T)]}{\epsilon^2} \geq 1 - \frac{(|z|_{\max}^j)^2 \sigma^2}{T \epsilon^2}. \quad (64)$$

Consequently, $\forall i, j \in \mathcal{V}$, $\Pr\{|\Xi_{ij}(T)| < \epsilon\} \geq 1 - \frac{(|z|_{\max}^j)^2 \sigma^2}{T \epsilon^2} \geq 1 - \frac{(|z|_{\max}^j)^2 \sigma^2}{T \epsilon^2}$, which completes the first statement.

Next, if $|z|_m < \infty, \forall T \in \mathbb{N}^+$, when $T \rightarrow \infty$, it yields that

$$\lim_{T \rightarrow \infty} \Pr\{|\Xi_{ij}(T)| < \epsilon\} = 1. \quad (65)$$

Finally, in the matrix form, (65) is equivalent to $\Pr\{\lim_{T \rightarrow \infty} \Xi(T) = \mathbf{0}\} = 1$. The proof is completed. \square

B. Proof of Theorem 1

Proof. Substitute (18) into $\Sigma_1(T)$ and it follows that

$$\begin{aligned} \Sigma_1(T) &= \frac{1}{T} (Y_T^+) (Y_T^-)^\top = \frac{1}{T} \sum_{t=1}^T y_t y_{t-1}^\top \\ &= \frac{W}{T} \sum_{t=1}^T y_{t-1} y_{t-1}^\top + \frac{1}{T} \sum_{t=1}^T (\theta_{t-1} + v_t - W v_{t-1}) y_{t-1}^\top. \end{aligned} \quad (66)$$

Note that when $W \in \mathcal{S}_a$, $\lim_{t \rightarrow \infty} \|y_t\| < \infty$ holds almost surely. Since θ_{t-1} and v_t are independent of y_t , applying Lemma 2 on $\Sigma_1(T)$, it yields that

$$\lim_{T \rightarrow \infty} \frac{1}{T} \sum_{t=1}^T \theta_{t-1} y_{t-1}^\top = \mathbf{0}, \quad \lim_{T \rightarrow \infty} \frac{1}{T} \sum_{t=1}^T v_t y_{t-1}^\top = \mathbf{0}. \quad (67)$$

Recalling v_{t-1} is independent of x_{t-1} , it follows that

$$\lim_{T \rightarrow \infty} \frac{1}{T} \sum_{t=1}^T v_{t-1} y_{t-1}^\top = \lim_{T \rightarrow \infty} \frac{1}{T} \sum_{t=1}^T v_{t-1} (x_{t-1} + v_{t-1})^\top = \sigma_v^2 I.$$

Then, one infers that

$$\lim_{T \rightarrow \infty} \Sigma_1(T) = W \left(\lim_{T \rightarrow \infty} \Sigma_0(T) - \sigma_v^2 I \right). \quad (68)$$

Hence, the proof is completed. \square

C. Proof of Theorem 2

Proof. Without losing generality, we first consider $\Sigma_0(T)$. Substituting the expanded form (6) of y_t into $y_t y_t^\top$, one obtains

$$y_t y_t^\top = (W^t x_0 + \eta_t) (W^t x_0 + \eta_t)^\top, \quad (69)$$

where $\eta_t = \sum_{m=1}^t W^{m-1} \theta_{t-m} + v_t$ and $\eta_0 = v_0$. Then, $y_t y_t^\top$ is expanded as

$$y_t y_t^\top = \underbrace{W^t x_0 x_0^\top (W^t)^\top}_{Q_1^t} + \underbrace{W^t x_0 \eta_t^\top}_{Q_2^t} + \underbrace{\eta_t x_0^\top (W^t)^\top}_{Q_3^t} + \underbrace{\eta_t \eta_t^\top}_{Q_4^t}. \quad (70)$$

Based on (70), the proof is equivalent to separately find the average of the summation of each part in (70) along the observation horizon T .

First, consider taking the average of all $\{Q_1^t\}_{t=0}^{T-1}$. Note that when $W \in \mathcal{S}_a \cup \mathcal{S}_m$, $W^\infty x_0$ converge to a constant vector. Therefore, it yields that

$$\begin{aligned} \lim_{T \rightarrow \infty} \frac{1}{T} \sum_{t=0}^{T-1} Q_1^t &= \lim_{T \rightarrow \infty} \frac{1}{T} \sum_{t=0}^{T-1} W^t x_0 x_0^\top (W^t)^\top \\ &= W^\infty x_0 x_0^\top (W^\infty)^\top. \end{aligned} \quad (71)$$

Next, consider $\frac{1}{T} \sum_{t=0}^{T-1} Q_2^t = \frac{1}{T} \sum_{t=0}^{T-1} W^t x_0 \eta_t^\top$. Since η_t is a typical linear combination of Gaussian noises $\{\theta_m\}_{m=0}^{t-1}$ and v_t , and is independent of $W^t x_0$, by Lemma 2, one infers that

$$\lim_{T \rightarrow \infty} \frac{1}{T} \sum_{t=0}^{T-1} Q_2^t = \lim_{T \rightarrow \infty} \frac{1}{T} \sum_{t=0}^{T-1} (W^t x_0) \eta_t^\top = \mathbf{0}. \quad (72)$$

The average of all $\{Q_3^t\}_{t=0}^{T-1}$ is likewise, i.e.,

$$\lim_{T \rightarrow \infty} \frac{1}{T} \sum_{t=0}^{T-1} Q_3^t = \mathbf{0}. \quad (73)$$

Then, focus on the calculation of $\frac{1}{T} \sum_{t=0}^{T-1} Q_4^t$. Since $\mathbb{E}(\theta_t \theta_t^\top) = \sigma_\theta^2 I$ and $\mathbb{E}(v_t v_t^\top) = \sigma_v^2 I$, one can divide Q_4^t as

$$\begin{aligned} Q_4^t &= \sum_{m=0}^t \left(W^{m-1} \theta_{t-m} (v_t + \sum_{\substack{m_1=0, \\ m_1 \neq m}}^t \theta_{t-m_1}^\top (W^{m_1-1})^\top) \right) \\ &\quad + v_t \left(\sum_{m_1=0}^t \theta_{t-m_1}^\top (W^{m_1-1})^\top \right) \\ &\quad + \sum_{m=0}^t W^{m-1} \theta_{t-m} \theta_{t-m}^\top (W^{m-1})^\top + v_t v_t^\top. \end{aligned} \quad (74)$$

Consider the first term in Q_4^t . For simple expression, define

$$\theta_t^a(m) = W^{m-1} \theta_{t-m}, \quad \theta_t^b(m) = \sum_{\substack{m_1=0, \\ m_1 \neq m}}^t W^{m_1-1} \theta_{t-m_1}. \quad (75)$$

As $W \in \mathcal{S}_a$, one can infer that $\lim_{t \rightarrow \infty} \|\theta_t^b(m)\| < \infty$. Therefore, by the famous Lebesgue's dominated convergence theorem and Lemma 2, it follows that with probability one

$$\begin{aligned} \lim_{T \rightarrow \infty} \frac{1}{T} \sum_{t=1}^T \sum_{m=0}^t \theta_t^a(m) (\theta_t^b(m))^\top \\ = \lim_{T \rightarrow \infty} \frac{\sum_{m=0}^t \theta_t^a(m) (\theta_t^b(m))^\top}{T} = \mathbf{0}. \end{aligned} \quad (76)$$

Likewise, for the second term in (74), it also holds that

$$\lim_{T \rightarrow \infty} \frac{1}{T} \sum_{t=0}^{T-1} v_t \left(\sum_{m_1=0}^t \theta_{t-m_1}^\top (W^{m_1-1})^\top \right) = \mathbf{0}. \quad (77)$$

As for the last two parts in (74), recalling $\mathbb{D}[\theta_t] = \sigma_\theta^2 I$ and $\mathbb{D}[v_t] = \sigma_v^2 I$, and one infers that

$$\begin{aligned} & \lim_{T \rightarrow \infty} \frac{\sum_{t=0}^{T-1} \sum_{m=0}^t W^{m-1} \theta_{t-m} \theta_{t-m}^\top (W^{m-1})^\top + \sum_{t=0}^{T-1} v_t v_t^\top}{T} \\ &= \sum_{t=0}^{\infty} W^t \lim_{T \rightarrow \infty} \left(\sum_{m=0}^{T-t} \theta_{T-m} \theta_{T-m}^\top / T \right) (W^t)^\top + \sigma_v^2 I \\ &= \sigma_\theta^2 \sum_{t=0}^{\infty} W^t (W^t)^\top + \sigma_v^2 I = \lim_{T \rightarrow \infty} \frac{1}{T} \sum_{t=0}^{T-1} Q_4^t. \end{aligned} \quad (78)$$

Finally, taking (71)-(73) and (78) into $\lim_{T \rightarrow \infty} \Sigma_0(T)$ implies that

$$\begin{aligned} \lim_{T \rightarrow \infty} \Sigma_0(T) &= \lim_{T \rightarrow \infty} \frac{1}{T} \sum_{t=0}^{T-1} (Q_1^t + Q_2^t + Q_3^t + Q_4^t) \\ &= \lim_{T \rightarrow \infty} \frac{1}{T} \sum_{t=0}^{T-1} (Q_1^t + Q_4^t) \\ &= W^\infty x_0 x_0^\top (W^\infty)^\top + \sigma_\theta^2 \sum_{t=0}^{\infty} W^t (W^t)^\top + \sigma_v^2 I \\ &= R_0^x(\infty) + \sigma_v^2 I. \end{aligned} \quad (79)$$

The proof of $\Sigma_1(\infty) = R_1^x(\infty) + \sigma_v^2 W$ is likewise and omitted here. The proof is completed. \square

D. Proof of Theorem 4

Proof. We proceed this proof based on the analysis in Theorem 2. The key point is to reveal the growing characteristic of the deviation norm in terms of T . Recall $\eta_t = \sum_{m=1}^t W^{m-1} \theta_{t-m} + v_t$ ($\eta_0 = v_0$), and the deviation matrix $(\Sigma_0(T) - R_0^x(T) - \sigma_v^2 I)$ is expanded as

$$\begin{aligned} & \Sigma_0(T) - R_0^x(T) - \sigma_v^2 I \\ &= \frac{1}{T} \left(\sum_{t=0}^{T-1} (W^t x_0) \eta_t^\top + \sum_{t=0}^{T-1} \eta_t x_0^\top (W^t)^\top + \sum_{t=0}^{T-1} \eta_t \eta_t^\top \right) - \sigma_\theta^2 \sum_{t=0}^{T-1} W^t (W^t)^\top \\ &+ \frac{1}{T} \sum_{t=0}^{T-1} W^t x_0 x_0^\top (W^t)^\top - W^{T-1} x_0 x_0^\top (W^{T-1})^\top - \sigma_v^2 I. \end{aligned} \quad (80)$$

Due to $W \in \mathcal{S}_m$, $\lim_{m \rightarrow \infty} W^m$ exists, i.e., $\|W^m\|^{ij} < \infty$, $\forall m \in \mathbb{R}^+$. Therefore, the spectral norm of the last three terms in (80) is bounded. Then, the major focus is laid on the first three terms. Considering an element-wise analysis of $W^{m-1} \theta_{t-m}$, the noise variance in every dimension is given by

$$\mathbb{D}([W^{m-1} \theta_{t-m}]^i) = \sigma_\theta^2 \sum_{j=1}^n ([W^{m-1}]^{ij})^2, \forall i \in \mathcal{V}. \quad (81)$$

Since $[W^m]^{ij}$ is strictly bounded, there exists a n -dimension state vector \tilde{x} and a Gaussian noise $\tilde{\theta} \sim N(0, \tilde{\sigma}^2 I)$ such that

$$\|W^m x_0\| \leq \|\tilde{x}\| < \infty, \mathbb{D}([W^{m-1} \theta_{t-m}]^i) \leq \mathbb{D}(\tilde{\theta}^{[i]}) = \tilde{\sigma}^2. \quad (82)$$

Based on (82), we define a revised version of η_t by $\tilde{\eta}_t = \sum_{m=1}^t \tilde{\theta}_t + v_t$ ($\tilde{\eta}_0 = v_0$), and the alternative of the first three terms in (80) is given by

$$E_\theta = \frac{1}{T} \left(\underbrace{\tilde{x} \sum_{t=0}^{T-1} \tilde{\eta}_t^\top}_{J_1(T)} + \underbrace{\sum_{t=0}^{T-1} \tilde{\eta}_t \tilde{x}^\top}_{J_2(T)} + \underbrace{\sum_{t=1}^T \tilde{\eta}_t \tilde{\eta}_t^\top}_{J_3(T)} \right). \quad (83)$$

In the sequel, we turn to analyze the the asymptotic performance of $\|E_\theta\|$ to demonstrate that of $\|\Sigma_0(T) - R_0^x(T) - \sigma_v^2 I\|$.

First, look at the each entry in $J_1^{[ij]}(T) = \tilde{x}^{[i]} \sum_{t=0}^{T-1} \tilde{\eta}_t^{[j]}$, which satisfies

$$\mathbb{E}\{J_1^{[ij]}(T)\} = 0, \mathbb{D}\{J_1^{[ij]}(T)\} = (\tilde{x}^{[i]})^2 \tilde{\sigma}^2 T. \quad (84)$$

By the Chebyshev inequality, given $0 < \delta < 1$, one has

$$\Pr\{|J_1^{[ij]}(T)| \leq \sqrt{\frac{T}{\delta}} \tilde{\sigma} |\tilde{x}^{[i]}|\} \geq 1 - \delta. \quad (85)$$

Therefore, it yields that at least with probability $1 - \delta$,

$$|J_1^{[ij]}(T)/T| \leq \sqrt{\frac{1}{T\delta}} \tilde{\sigma} \tilde{x}^m, \forall i, j \in \mathcal{V}, \quad (86)$$

where $\tilde{x}^m = \max\{|\tilde{x}^{[i]}|, i \in \mathcal{V}\}$. Note that $J_1(T) = J_2^\top(T)$, thus the bound in (86) also applies to $J_2^{[ij]}(T)$.

Next, consider the entries in $J_3(T)$. Since the autocorrelation of $\{\tilde{\theta}_t\}_{t=1}^T$ and $\{\tilde{v}_t\}_{t=1}^T$ are involved, it can be further expanded as

$$\begin{aligned} J_3(T) &= \sum_{t=0}^{T-1} \left(\sum_{t_1=0}^t \sum_{\substack{t_2=0, \\ t_2 \neq t_1}}^t \tilde{\theta}_{t_1} \tilde{\theta}_{t_2}^\top + \sum_{t_1=0}^t \tilde{\theta}_{t_1} \tilde{\theta}_{t_1}^\top \right. \\ &\quad \left. + \sum_{t_1=0}^t \tilde{\theta}_{t_1} v_{t_1}^\top + \sum_{t_1=0}^t \tilde{v}_{t_1} \theta_{t_1}^\top + v_t v_t^\top \right). \end{aligned} \quad (87)$$

Recall that the product of two independent Gaussian variable also subjects to Gaussian distribution, thus it follows that

$$\begin{cases} \mathbb{E}\{(\tilde{\theta}_{t_1} \tilde{\theta}_{t_2}^\top)^{[ij]}\} = 0, & \mathbb{E}\{(\tilde{\theta}_{t_1} \tilde{v}_{t_1}^\top)^{[ij]}\} = 0, \\ \mathbb{D}\{(\tilde{\theta}_{t_1} \tilde{\theta}_{t_2}^\top)^{[ij]}\} = \frac{\tilde{\sigma}^2}{2}, & \mathbb{D}\{(\tilde{\theta}_{t_1} \tilde{v}_{t_1}^\top)^{[ij]}\} = \frac{\tilde{\sigma}^2 \sigma_v^2}{\tilde{\sigma}^2 + \sigma_v^2}, \end{cases} \quad (88)$$

where $t_1 \neq t_2$. Applying the Chebyshev inequality again, for each entry in $J_3(T)$, one has with probability at least $1 - \delta$

$$\begin{aligned} |J_3^{[ij]}(T)| &\leq \sqrt{\frac{\sum_{t=1}^{T-1} t(t+1)}{2\delta}} \tilde{\sigma} + 2 \sqrt{\frac{\sum_{t=1}^T t}{\delta}} \sqrt{\frac{\tilde{\sigma}^2 \sigma_v^2}{\tilde{\sigma}^2 + \sigma_v^2}} \\ &\quad + \left(\sum_{t=1}^T t \right) \frac{\tilde{\sigma}^2}{\delta} + \frac{T \sigma_v^2}{\delta}. \end{aligned} \quad (89)$$

Then, divide T into $J_3(T)$ and do series summation, yielding

$$\begin{aligned} \left| \frac{J_3^{[ij]}(T)}{T} \right| &\leq \sqrt{\frac{2T^3 - 3T^2 + T}{12T^2 \delta}} \tilde{\sigma} + \sqrt{\frac{2T^2 - T}{T^2 \delta}} \sqrt{\frac{\tilde{\sigma}^2 \sigma_v^2}{\tilde{\sigma}^2 + \sigma_v^2}} \\ &\quad + \frac{T+1}{2\delta} \tilde{\sigma}^2 + \frac{\sigma_v^2}{\delta} \triangleq \bar{J}(T). \end{aligned} \quad (90)$$

Finally, utilizing the inequality $\|B\| \leq \|B\|_F \leq \sum_{i,j \in \mathcal{V}} \|B^{[ij]}\|$ ($B \in \mathbb{R}^{n \times n}$), it is induced that with probability at least $1 - \delta$

$$\left\| \frac{J_3(T)}{T} \right\| \leq n^2 \bar{J}(T) \sim \mathcal{O}\left(\frac{T}{\delta}\right). \quad (91)$$

Note that $\|R_0^x(T)\| = \|\sigma_\theta^2 \sum_{t=0}^{T-1} W^t (W^t)^\top\| \leq T \sigma_\theta^2$, then there exists a possibility that the part with factor T in $\frac{J_3(T)}{T}$ can be offset with $R_0^x(T) + \sigma_v^2 I$, i.e.,

$$\left\| R_0^x(T) + \sigma_v^2 I - \frac{\sum_{t=0}^{T-1} \sum_{m=0}^t W^{m-1} \theta_{t-m} \theta_{t-m}^\top (W^{m-1})^\top}{T} \right\| \xrightarrow{T \rightarrow \infty} \mathcal{O}(1). \quad (92)$$

However, even if the situation in (92) happens, by (90) one can infer that $\|\Sigma_0(\infty) - R_0^x(\infty) - \sigma_v^2 I\| \sim \mathcal{O}(\sqrt{T})$ holds, indicating the deviation still goes to infinity with the increase of T . Hence, the spectral norm of the deviation (80) at least satisfies $\mathcal{O}(\sqrt{T})$, which completes the proof. \square

E. Proof of Theorem 5

Proof. The proof is rather similar to that of Theorem 2. The key idea is to prove the upper bounds of the estimation error, by leveraging the concentration measure in Gaussian space. Since $\hat{W}_o = Y_T^+ (Y_T^-)^\top (Y_T^- (Y_T^-)^\top)^{-1}$, one obtains the estimation error matrix E_W by

$$E_W = \hat{W}_o - W = (\Theta_T + \Upsilon_T^+ - W \Upsilon_T^-) (Y_T^-)^\top \Sigma_T^{-1}. \quad (93)$$

Due to $\|W\| \leq 1$ and $Y_T^- = X_T^- + \Upsilon_T^-$ holds, $\|E_W\|$ is upper bounded by

$$\begin{aligned} \|E_W\| \leq & \|\Theta_T (Y_T^-)^\top \Sigma_T^{-1}\| + \|\Upsilon_T^+ (Y_T^-)^\top \Sigma_T^{-1}\| \\ & + \|\Upsilon_T^- (X_T^-)^\top \Sigma_T^{-1}\| + \|\Upsilon_T^- (\Upsilon_T^-)^\top \Sigma_T^{-1}\|. \end{aligned} \quad (94)$$

Then, the proof is turned to bound each term of the right-hand side in (94) individually.

- *Part 1: Upper Bounding $\|\Theta_T (Y_T^-)^\top \tilde{\Sigma}_T^{-1}\|$.*

Utilizing $0 \prec \Sigma_{dn} \preceq \tilde{\Sigma}_T \preceq \Sigma_{up}$, it yields that

$$\Sigma_T + \Sigma_{dn} \preceq 2\Sigma_T \implies (\Sigma_T + \Sigma_{dn})^{-1} \succeq \Sigma_T^{-1}/2, \quad (95)$$

$$\|(\Sigma_T + \Sigma_{dn})^{-\frac{1}{2}}\| \geq \|\Sigma_T^{-\frac{1}{2}}\|/\sqrt{2}. \quad (96)$$

By Lemma 4, one has probability at least $1 - \delta$ that

$$\|\Theta_T \tilde{\Sigma}_T^{-\frac{1}{2}}\| \leq \sqrt{16n \log \left(\frac{5 \det(\tilde{\Sigma}_T \Sigma_{dn}^{-1} + I)^{\frac{1}{2n}}}{\delta^{1/n}} \right)}. \quad (97)$$

Further, substitute $\tilde{\Sigma}_T \preceq \Sigma_{up}$ into in (97) and use $\|\tilde{\Sigma}_T^{-\frac{1}{2}}\| \leq \frac{1}{\sqrt{\rho_{\min}(\Sigma_{dn})}}$ and one obtains

$$\|\Theta_T \tilde{\Sigma}_T^{-1}\| \leq \frac{1}{\sqrt{\rho_{\min}(\Sigma_{dn})}} \sqrt{16n \log \left(\frac{5 \det(\Sigma_{up} \Sigma_{dn}^{-1} + I)^{\frac{1}{2n}}}{\delta^{1/n}} \right)}. \quad (98)$$

- *Part 2: Upper Bounding $\|\Upsilon_T^- (Y_T^-)^\top \tilde{\Sigma}_T^{-1}\|$.*

Since $\{v_t, y_{t-1}\}_{t=1}^T$ are dependent with other, thus the same upper of (98) also applies to $\|\Upsilon_T^+ (Y_T^-)^\top \tilde{\Sigma}_T^{-1}\|$.

- *Part 3: Upper Bounding $\|\Upsilon_T^- (X_T^-)^\top \tilde{\Sigma}_T^{-1}\|$.*

Note that $Y_T^- (Y_T^-)^\top = X_T^- (X_T^-)^\top + \tilde{V}$, where $\tilde{V} = X_T^- (\Upsilon_T^-)^\top + \Upsilon_T^- (X_T^-)^\top + \Upsilon_T^- (\Upsilon_T^-)^\top \succ \mathbf{0}$. Then, one can directly apply Lemma 4 and obtain

$$\|\Sigma_T^{-1/2} X_T^- \Upsilon_T^-\| \leq \sqrt{8n \log \left(\frac{5 \det(\Sigma_T \tilde{V}^{-1} + I)^{\frac{1}{2n}}}{\delta^{1/n}} \right)}. \quad (99)$$

Further taking $\Sigma_{dn} \preceq X_T^- (X_T^-)^\top \preceq \tilde{\Sigma}_T \preceq \Sigma_{up}$ and (99) into $\|\Sigma_T^{-1} X_T^- \Upsilon_T^-\|$, a loose upper bound is given by

$$\|\Sigma_T^{-1} X_T^- \Upsilon_T^-\| \leq \frac{1}{\sqrt{\rho_{\min}(\Sigma_{dn})}} \sqrt{9n \log \left(\frac{5 \det(\Sigma_{up} \Sigma_{dn}^{-1} + I)^{\frac{1}{2n}}}{\delta^{1/n}} \right)}. \quad (100)$$

- *Part 4: Upper Bounding $\|\Upsilon_T^- (\Upsilon_T^-)^\top \tilde{\Sigma}_T^{-1}\|$.*

Applying Lemma 3 to $\Upsilon_T^- (\Upsilon_T^-)^\top$, and it is not difficult to obtain that with probability at least $1 - 2 \exp(-r^2/2)$

$$(\sqrt{T} - \sqrt{n} - r)^2 \sigma_v^2 I \preceq \Upsilon_T^- (\Upsilon_T^-)^\top \preceq (\sqrt{T} + \sqrt{n} + r)^2 \sigma_v^2 I. \quad (101)$$

Let $r = \sqrt{2 \log \frac{2}{\delta}}$ and focus on the right side of $\Upsilon_T^- (\Upsilon_T^-)^\top$. When $T \geq T_\delta = (\sqrt{n} + \sqrt{2 \log \frac{2}{\delta}})^2 / (\sqrt{5}/2 - 1)^2$, one has with probability $1 - \delta$ that

$$\frac{3T\sigma_v^2}{4} I \preceq \Upsilon_T^- (\Upsilon_T^-)^\top \preceq \frac{5T\sigma_v^2}{4} I. \quad (102)$$

It follows from (102) and $\|\tilde{\Sigma}_T^{-1}\| \leq 1/\rho_{\min}(\Sigma_{dn})$ that

$$\|\Upsilon_T^- (\Upsilon_T^-)^\top \tilde{\Sigma}_T^{-1}\| \leq \|\Upsilon_T^- (\Upsilon_T^-)^\top\| \|\tilde{\Sigma}_T^{-1}\| \leq \frac{5T\sigma_v^2}{4\rho_{\min}(\Sigma_{dn})}. \quad (103)$$

Finally, combining the upper bounds of four parts leads to

$$\|E_W\| \leq \frac{\left(11 \sqrt{n \log \left(\frac{5 \det(\Sigma_{up} \Sigma_{dn}^{-1} + I)^{\frac{1}{2n}}}{\delta^{1/n}} \right)} + \frac{5T\sigma_v^2}{4\sqrt{\rho_{\min}(\Sigma_{dn})}} \right)}{\sqrt{\rho_{\min}(\Sigma_{dn})}}, \quad (104)$$

which completes the proof. \square

F. Proof of Theorem 6

Proof. The key point of this proof is to provide a group of explicit Σ_{dn} and Σ_{up} about T . First we focus on analyzing the case of \hat{W}_o and then easily extend the analysis to that of \hat{W}_C . Note that we are not interested in finding the best Σ_{dn} and Σ_{up} rather illustrate their existence.

For Σ_{dn} , it has been proved that (in Proposition 8.5. [52]) there exists some scalar functions α_n that depends only on n , such that $\tilde{\Sigma}_T \succeq \alpha_n T I$. Then, it follows that

$$\|\Sigma_{dn}^{-1}\| \leq \frac{1}{\rho_{\min}(\alpha_n T I)} = \frac{1}{\alpha_n T} \sim \mathcal{O}\left(\frac{1}{T}\right). \quad (105)$$

For Σ_{up} , note that the following inevitable always holds

$$\tilde{\Sigma}_T \preceq \text{tr} \left(\sum_{t=0}^{T-1} y_t y_t^\top \right) I = \Sigma_{up} \quad (106)$$

When $W \in \mathcal{S}_m$, part of the upper bound of $[\Sigma_{up}]^{ij}$ is given by (89) in the proof of Theorem 4, demonstrating $[\sum_{t=0}^{T-1} y_t y_t^\top]^{ij} \sim \mathcal{O}(T^2)$. When $W \in \mathcal{S}_a$, it is also proved in Theorem 2 that $\|\tilde{\Sigma}_T/T\| \xrightarrow{T \rightarrow \infty} \|\sigma_\theta^2 \sum_{t=0}^{\infty} W^t (W^t)^\top + \sigma_v^2 I\|$, which is strictly bounded. Therefore, one can easily infer that

$$\|\Sigma_{up}\| \sim \begin{cases} \mathcal{O}(T^2), & \text{if } W \in \mathcal{S}_m, \\ \mathcal{O}(T), & \text{if } W \in \mathcal{S}_a. \end{cases} \quad (107)$$

Combine the two factors (105) and (107), and it follows that

$$\det(\Sigma_{up} \Sigma_{dn}^{-1} + I) \sim \begin{cases} \mathcal{O}(T), & \text{if } W \in \mathcal{S}_m, \\ \mathcal{O}(1), & \text{if } W \in \mathcal{S}_a. \end{cases} \quad (108)$$

Taking (105) and (108) into (11) $\sqrt{n \log(\frac{5 \det(\Sigma_{up} \Sigma_{dn}^{-1} + I)}{\delta^{1/n}})^{\frac{1}{2n}} + \frac{5T\sigma_v}{4\sqrt{\rho_{\min}(\Sigma_{dn})}}}) / \sqrt{\rho_{\min}(\Sigma_{dn})}$ yields the relationship given by (31), which completes the proof of the first statement.

Next, consider the the non-asymptotic bound of $\|\hat{W}_c - W\|$. Let $\Sigma_{T,\sigma_v} = T\Sigma_0(T-1) - T\sigma_v^2 W$, and the causality-based estimator (20) is rewritten as

$$\hat{W}_c = Y_T^+ (Y_T^-)^\top \Sigma_{T,\sigma_v}^{-1}. \quad (109)$$

Then, the inference error is given by

$$\begin{aligned} \hat{W}_c - W &= (\Theta_T + \Upsilon_T^+ - W \Upsilon_T^-) (Y_T^-)^\top \Sigma_{T,\sigma_v}^{-1} + T\sigma_v^2 W \Sigma_{T,\sigma_v}^{-1} \\ &= (\Theta_T + \Upsilon_T^+)(Y_T^-)^\top \Sigma_{T,\sigma_v}^{-1} - W \Upsilon_T^- (X_T^-)^\top \Sigma_{T,\sigma_v}^{-1} \\ &\quad + W(T\sigma_v^2 I - \Upsilon_T^- (\Upsilon_T^-)^\top) \Sigma_{T,\sigma_v}^{-1}. \end{aligned} \quad (110)$$

Consequently, the upper bound is given by

$$\begin{aligned} \|\hat{W}_c - W\| &\leq \|\Theta_T (Y_T^-)^\top \Sigma_{T,\sigma_v}^{-1}\| + \|\Upsilon_T^+ (Y_T^-)^\top \Sigma_{T,\sigma_v}^{-1}\| \\ &\quad + \|\Upsilon_T^- (X_T^-)^\top \Sigma_{T,\sigma_v}^{-1}\| + \|(T\sigma_v^2 I - \Upsilon_T^- (\Upsilon_T^-)^\top) \Sigma_{T,\sigma_v}^{-1}\|. \end{aligned} \quad (111)$$

Note that the first three terms in (111) share the same upper bound forms as $\|\Theta_T (Y_T^-)^\top \Sigma_T^{-1}\|$, $\|\Upsilon_T^+ (Y_T^-)^\top \Sigma_T^{-1}\|$ and $\|\Upsilon_T^- (X_T^-)^\top \Sigma_T^{-1}\|$ in $\|\hat{W}_o - W\|$. The proof is similar to that of Theorem 5 and is omitted here. As for the last term in RHS of (111), one has with high probability that

$$\lim_{T \rightarrow \infty} \|T\sigma_v^2 I - \Upsilon_T^- (\Upsilon_T^-)^\top\|/T = 0. \quad (112)$$

Therefore, the upper bound of $\|\hat{W}_c - W\|$ is determined by the first three terms in (111), which converge to zero as $T \rightarrow \infty$. The second statement in Theorem 6 is proved. \square

G. Proof of Theorem 7

Proof. The proof consists of two steps. First, we prove the decision threshold z_0 is given by $z_0 = \frac{w_{ij}e^j}{2}$. Then, we demonstrate the critical excitation magnitude under the z_0 .

For simplicity without losing generality, we begin with the case where the excitation input $e^j > 0$. Note that ω^i is a continuous random variable, the likelihood ratio $l_r(z)$ in the test is given by

$$l_r(z) = \frac{f_\omega(z|H_1)}{f_\omega(z|H_0)}, \quad (113)$$

where $f_\omega(\cdot)$ is the probability density function of ω^i . Due to the prior probabilities $\Pr(H_1) = \Pr(H_0)$, the decision threshold z_0 satisfies

$$l_r(z_0) = \frac{f_\omega(z_0|H_1)}{f_\omega(z_0|H_0)} = \frac{\Pr\{H_1\}}{\Pr\{H_0\}} = 1. \quad (114)$$

Since $w^i \sim N(0, \sigma_\omega^2)$, substituting $f_\omega(y) = \frac{1}{\sqrt{2\pi\sigma_\omega}} \exp(-\frac{y^2}{2\sigma_\omega^2})$ into (114), it yields that

$$l_r(z_0) = \frac{\exp(-\frac{(z_0 - w_{ij}e^j)^2}{2\sigma_\omega^2})}{\exp(-\frac{z_0^2}{2\sigma_\omega^2})} = 1. \quad (115)$$

It follows from (115) that $z_0^2 - (z_0 - w_{ij}e^j)^2 = 0$, leading to

$$z_0 = \frac{w_{ij}e^j}{2}. \quad (116)$$

Next, by the definition of δ_e , one has

$$\begin{aligned} \delta_e &= \Pr\{D_1|H_0\} + \Pr\{D_0|H_1\} = \int_{z_0}^{+\infty} \frac{1}{\sqrt{2\pi\sigma_\omega}} \exp(-\frac{z^2}{2\sigma_\omega^2}) dz \\ &\quad + \int_{-\infty}^{z_0} \frac{1}{\sqrt{2\pi\sigma_\omega}} \exp(-\frac{(z - w_{ij}e^j)^2}{2\sigma_\omega^2}) dz. \end{aligned} \quad (117)$$

Substitute $z = z' + \frac{w_{ij}e^j}{2} = z' + z_0$ into (117), yielding

$$\begin{aligned} \delta_e &= \Pr\{D_1|H_0\} + \Pr\{D_0|H_1\} \\ &= \int_0^{+\infty} \frac{1}{\sqrt{2\pi\sigma_\omega}} \exp(-\frac{(z' + z_0)^2}{2\sigma_\omega^2}) dz' \\ &\quad + \int_{-\infty}^0 \frac{1}{\sqrt{2\pi\sigma_\omega}} \exp(-\frac{(z' - z_0)^2}{2\sigma_\omega^2}) dz' \\ &= 2 \int_0^{+\infty} \frac{1}{\sqrt{2\pi\sigma_\omega}} \exp(-\frac{(z' + z_0)^2}{2\sigma_\omega^2}) dz' \\ &= 2 \int_{z_0}^{+\infty} \frac{1}{\sqrt{2\pi\sigma_\omega}} \exp(-\frac{z^2}{2\sigma_\omega^2}) dz. \end{aligned} \quad (118)$$

Note that $\int_{z_0}^{+\infty} \frac{1}{\sqrt{2\pi\sigma_\omega}} \exp(-\frac{z^2}{2\sigma_\omega^2}) dz = (1 - \text{erf}(\frac{z_0}{\sqrt{2\sigma_\omega}}))/2$, thus it yields that

$$\delta_e = 1 - \text{erf}(\frac{z_0}{\sqrt{2\sigma_\omega}}). \quad (119)$$

Substituting $z_0 = \frac{w_{ij}e^j}{2}$ and $\delta_e = \bar{\delta}_e$ into (119), we obtain

$$e^j = \frac{2\sqrt{2\sigma_\omega}}{w_{ij}} \text{erf}^{-1}(1 - \bar{\delta}_e). \quad (120)$$

The result is likewise when $e^j < 0$ due to the symmetry of Gaussian distribution. By the monotone increasing property of $\text{erf}(z)$, to guarantee $\delta_e \leq \bar{\delta}_e$, the excitation input must satisfy $|e^j| \geq \frac{2\sqrt{2\sigma_\omega}}{w_{ij}} \text{erf}^{-1}(1 - \bar{\delta}_e)$. The proof is completed. \square

H. Proof of Theorem 8

Proof. The proof consists of three steps. Denote the false alarm probability by $\delta_f(h) = \Pr\{D_1(h)|H_0(h)\}$ and the missed detection probability by $\delta_m(h) = \Pr\{D_0(h)|H_1(h)\}$. We first prove the critical excitation magnitude for identifying the neighbors within h -hops. Then, we find the lower and upper bounds of $\delta_f(l)$ and $\delta_d(l)$.

Based on the famous Neyman-Pearson rule, with a specified $\delta_f = \alpha$, one has

$$\alpha = \int_{z_0}^{+\infty} \frac{1}{\sqrt{2\pi}\sigma_\omega} \exp\left(-\frac{z^2}{2\sigma_\omega^2}\right) dz = \frac{(1 - \text{erf}\left(\frac{z_0}{\sqrt{2}\sigma_\omega}\right))}{2}. \quad (121)$$

It follows from (121) that

$$z_0 = \sqrt{2}\sigma_\omega \text{erf}^{-1}(1 - 2\alpha). \quad (122)$$

Due to the prior probabilities $\Pr\{H_1\} = \Pr\{H_0\}$ and based on Lemma 5, $z_0 = \frac{\Gamma_{ij}(h)e^j}{2}$ also holds at h -step response. Substituting it into (122), it yields that

$$e^j = \frac{2\sqrt{2}\sigma_\omega \text{erf}^{-1}(1 - 2\alpha)}{\Gamma_{ij}(h)}. \quad (123)$$

Next, note that $F_0(z, e^j)$ decreases with ze^j increasing. If the excitation input is designed such that

$$e_m^j = \frac{2\sqrt{2}\sigma \text{erf}^{-1}(1 - 2\alpha)}{\min\{\Gamma_{ij}(h), h = 1, \dots, n\}}, \quad (124)$$

then one infers that

$$\delta_f(l) = F_0(\Gamma_{ij}(l), e_m^j) \leq \alpha, \quad \forall 1 \leq l \leq h. \quad (125)$$

Meanwhile, recall the detection probability $\delta_d(h) = \Pr\{D_1(h)|H_1(h)\}$ is calculated by

$$\delta_d(h) = \int_{\frac{\Gamma_{ij}(h)e^j}{2}}^{\infty} \frac{1}{\sqrt{2\pi}\sigma_\omega} \exp\left(-\frac{(z - \Gamma_{ij}(h)e^j)^2}{2\sigma_\omega^2}\right) dz. \quad (126)$$

Since $\delta_d(h)$ increases with $\Gamma_{ij}(h)e_{\max}^j$ increasing, one has

$$F_1(\Gamma_{ij}^{\min}, e_m^j) \leq \delta_d(h) \leq F_1(\Gamma_{ij}^{\max}, e_m^j). \quad (127)$$

Finally, utilizing the Law of Total Probability, the probability that i is decided as member of $\mathcal{N}_{j,h}^{\text{out}}$ is calculated by

$$\begin{aligned} \Pr\{i \in \mathcal{N}_{j,h}^{\text{out}}\} &= \Pr\{D_1(h)|H_1(h)\} \Pr\{D_0(h-1)|H_0(h-1)\} \\ &\quad + \Pr\{D_1(h)|H_1(h)\} \Pr\{D_0(h-1)|H_1(h-1)\}. \end{aligned} \quad (128)$$

Substitute $\Pr\{D_0(h-1)|H_0(h-1)\} = 1 - \delta_f(h-1)$ and $\Pr\{D_0(h-1)|H_1(h-1)\} = 1 - \delta_d(h-1)$ into (128), and it yields that

$$\begin{aligned} \Pr\{i \in \mathcal{N}_{j,h}^{\text{out}}\} &= \delta_d(h)(2 - \delta_f(h-1) - \delta_d(h-1)) \\ &\geq F_1(\Gamma_{ij}^{\min}, e_m^j)(2 - \alpha - F_1(\Gamma_{ij}^{\max}, e_m^j)). \end{aligned} \quad (129)$$

The proof is completed. \square

REFERENCES

- [1] Y. Li and J. He, "Topology inference for networked dynamical systems: A causality and correlation perspective," in *60th IEEE Conference on Decision and Control*. submitted, 2021.
- [2] R. Olfati-Saber, J. A. Fax, and R. M. Murray, "Consensus and cooperation in networked multi-agent systems," *Proceedings of the IEEE*, vol. 95, no. 1, pp. 215–233, 2007.
- [3] M. Nokleby and W. U. Bajwa, "Stochastic optimization from distributed streaming data in rate-limited networks," *IEEE Transactions on Signal and Information Processing over Networks*, vol. 5, no. 1, pp. 152–167, 2018.
- [4] A. Ahmed and E. P. Xing, "Recovering time-varying networks of dependencies in social and biological studies," *Proceedings of the National Academy of Sciences*, vol. 106, no. 29, pp. 11878–11883, 2009.
- [5] R. P. Monti, P. Hellyer, D. Sharp, R. Leech, C. Anagnostopoulos, and G. Montana, "Estimating time-varying brain connectivity networks from functional MRI time series," *NeuroImage*, vol. 103, pp. 427–443, 2014.
- [6] C. Liu, J. He, S. Zhu, and C. Chen, "Dynamic topology inference via external observation for multi-robot formation control," in *2019 IEEE Pacific Rim Conference on Communications, Computers and Signal Processing (PACRIM)*. IEEE, 2019, pp. 1–6.
- [7] S. Mahdizadehaghdam, H. Wang, H. Krim, and L. Dai, "Information diffusion of topic propagation in social media," *IEEE Transactions on Signal and Information Processing over Networks*, vol. 2, no. 4, pp. 569–581, 2016.
- [8] M. Cheraghchi, A. Karbasi, S. Mohajer, and V. Saligrama, "Graph-constrained group testing," *IEEE Transactions on Information Theory*, vol. 58, no. 1, pp. 248–262, 2012.
- [9] M. Mardani, G. Mateos, and G. B. Giannakis, "Dynamic anomalography: Tracking network anomalies via sparsity and low rank," *IEEE Journal of Selected Topics in Signal Processing*, vol. 7, no. 1, pp. 50–66, 2013.
- [10] G. B. Giannakis, Y. Shen, and G. V. Karanikolas, "Topology identification and learning over graphs: Accounting for nonlinearities and dynamics," *Proceedings of the IEEE*, vol. 106, no. 5, pp. 787–807, 2018.
- [11] C. W. Granger, "Investigating causal relations by econometric models and cross-spectral methods," *Econometrica: Journal of the Econometric Society*, pp. 424–438, 1969.
- [12] A. Brovelli, M. Ding, A. Ledberg, Y. Chen, R. Nakamura, and S. L. Bressler, "Beta oscillations in a large-scale sensorimotor cortical network: Directional influences revealed by granger causality," *Proceedings of the National Academy of Sciences*, vol. 101, no. 26, pp. 9849–9854, 2004.
- [13] A. Santos, V. Matta, and A. H. Sayed, "Local tomography of large networks under the low-observability regime," *IEEE Transactions on Information Theory*, vol. 66, no. 1, pp. 587–613, 2020.
- [14] S. Segarra, A. G. Marques, G. Mateos, and A. Ribeiro, "Network topology inference from spectral templates," *IEEE Transactions on Signal and Information Processing over Networks*, vol. 3, no. 3, pp. 467–483, 2017.
- [15] M. T. Schaub, S. Segarra, and H.-T. Wai, "Spectral partitioning of time-varying networks with unobserved edges," in *2019 IEEE International Conference on Acoustics, Speech and Signal Processing (ICASSP)*. IEEE, 2019, pp. 4938–4942.
- [16] Y. Zhu, M. T. Schaub, A. Jadbabaie, and S. Segarra, "Network inference from consensus dynamics with unknown parameters," *IEEE Transactions on Signal and Information Processing over Networks*, vol. 6, pp. 300–315, 2020.
- [17] G. Karanikolas, G. B. Giannakis, K. Slavakis, and R. M. Leahy, "Multi-kernel based nonlinear models for connectivity identification of brain networks," in *2016 IEEE International Conference on Acoustics, Speech and Signal Processing (ICASSP)*. IEEE, 2016, pp. 6315–6319.
- [18] G. V. Karanikolas, O. Sporns, and G. B. Giannakis, "Multi-kernel change detection for dynamic functional connectivity graphs," in *2017 51st Asilomar Conference on Signals, Systems, and Computers*. IEEE, 2017, pp. 1555–1559.
- [19] S. Wang, E. D. Herzog, I. Z. Kiss, W. J. Schwartz, G. Bloch, M. Sebek, D. Granados-Fuentes, L. Wang, and J.-S. Li, "Inferring dynamic topology for decoding spatiotemporal structures in complex heterogeneous networks," *Proceedings of the National Academy of Sciences*, vol. 115, no. 37, pp. 9300–9305, 2018.
- [20] J. Friedman, T. Hastie, and R. Tibshirani, "Sparse inverse covariance estimation with the graphical lasso," *Biostatistics*, vol. 9, no. 3, pp. 432–441, 2008.
- [21] S. Segarra, M. T. Schaub, and A. Jadbabaie, "Network inference from consensus dynamics," in *2017 IEEE 56th Annual Conference on Decision and Control (CDC)*. IEEE, 2017, pp. 3212–3217.
- [22] N. Shahid, N. Perraudin, V. Kalofolias, G. Puy, and P. Vanderghenst, "Fast robust PCA on graphs," *IEEE Journal of Selected Topics in Signal Processing*, vol. 10, no. 4, pp. 740–756, 2016.
- [23] M. Onuki, S. Ono, M. Yamagishi, and Y. Tanaka, "Graph signal denoising via trilateral filter on graph spectral domain," *IEEE Transactions on Signal and Information Processing over Networks*, vol. 2, no. 2, pp. 137–148, 2016.
- [24] H. E. Egilmez, E. Pavez, and A. Ortega, "Graph learning from data under Laplacian and structural constraints," *IEEE Journal of Selected Topics in Signal Processing*, vol. 11, no. 6, pp. 825–841, 2017.
- [25] V. N. Ioannidis, Y. Shen, and G. B. Giannakis, "Semi-blind inference of topologies and dynamical processes over dynamic graphs," *IEEE Transactions on Signal Processing*, vol. 67, no. 9, pp. 2263–2274, 2019.

[26] A. Tsiamis and G. J. Pappas, "Finite sample analysis of stochastic system identification," in *2019 IEEE 58th Conference on Decision and Control (CDC)*. IEEE, 2019, pp. 3648–3654.

[27] S. Oymak and N. Ozay, "Non-asymptotic identification of LTI systems from a single trajectory," in *2019 American control conference (ACC)*. IEEE, 2019, pp. 5655–5661.

[28] C. J. Quinn, N. Kiyavash, and T. P. Coleman, "Directed information graphs," *IEEE Transactions on Information Theory*, vol. 61, no. 12, pp. 6887–6909, 2015.

[29] J. Etesami and N. Kiyavash, "Measuring causal relationships in dynamical systems through recovery of functional dependencies," *IEEE Transactions on Signal and Information Processing over Networks*, vol. 3, no. 4, pp. 650–659, 2017.

[30] R. Bowden and D. Veitch, "Finding the right tree: Topology inference despite spatial dependences," *IEEE Transactions on Information Theory*, vol. 64, no. 6, pp. 4594–4609, 2018.

[31] X. Dong, D. Thanou, P. Frossard, and P. Vandergheynst, "Learning Laplacian matrix in smooth graph signal representations," *IEEE Transactions on Signal Processing*, vol. 64, no. 23, pp. 6160–6173, 2016.

[32] B. Pasdeloup, V. Gripon, G. Mercier, D. Pastor, and M. G. Rabbat, "Characterization and inference of graph diffusion processes from observations of stationary signals," *IEEE Transactions on Signal and Information Processing over Networks*, 2017.

[33] D. Hayden, Y. Yuan, and J. Gonçalves, "Network identifiability from intrinsic noise," *IEEE Transactions on Automatic Control*, vol. 62, no. 8, pp. 3717–3728, 2017.

[34] S. Shahrampour and V. M. Preciado, "Topology identification of directed dynamical networks via power spectral analysis," *IEEE Transactions on Automatic Control*, vol. 60, no. 8, pp. 2260–2265, 2014.

[35] ———, "Reconstruction of directed networks from consensus dynamics" in *2013 American Control Conference*. IEEE, 2013, pp. 1685–1690.

[36] V. Matta and A. H. Sayed, "Consistent tomography under partial observations over adaptive networks," *IEEE Transactions on Information Theory*, vol. 65, no. 1, pp. 622–646, 2019.

[37] G. Mateos, S. Segarra, A. G. Marques, and A. Ribeiro, "Connecting the dots: Identifying network structure via graph signal processing," *IEEE Signal Processing Magazine*, vol. 36, no. 3, pp. 16–43, 2019.

[38] S. Zhou, J. Lafferty, and L. Wasserman, "Time varying undirected graphs," *Machine Learning*, vol. 80, no. 2-3, pp. 295–319, 2010.

[39] A. J. Gibberd and J. D. Nelson, "High dimensional changepoint detection with a dynamic graphical lasso," in *2014 IEEE International Conference on Acoustics, Speech and Signal Processing (ICASSP)*. IEEE, 2014, pp. 2684–2688.

[40] E. Fox, E. Sudderth, M. Jordan, and A. Willsky, "Nonparametric Bayesian learning of switching linear dynamical systems," *Advances in Neural Information Processing Systems*, vol. 21, pp. 457–464, 2008.

[41] B. Baingana, G. Mateos, and G. B. Giannakis, "Proximal-gradient algorithms for tracking cascades over social networks," *IEEE Journal of Selected Topics in Signal Processing*, vol. 8, no. 4, pp. 563–575, 2014.

[42] B. Baingana and G. B. Giannakis, "Tracking switched dynamic network topologies from information cascades," *IEEE Transactions on Signal Processing*, vol. 65, no. 4, pp. 985–997, 2016.

[43] V. Kalofolias, A. Loukas, D. Thanou, and P. Frossard, "Learning time varying graphs," in *2017 IEEE International Conference on Acoustics, Speech and Signal Processing (ICASSP)*. IEEE, 2017, pp. 2826–2830.

[44] D. Hallac, Y. Park, S. Boyd, and J. Leskovec, "Network inference via the time-varying graphical Lasso," in *Proceedings of the 23rd ACM SIGKDD International Conference on Knowledge Discovery and Data Mining*, 2017, pp. 205–213.

[45] L. Peel and A. Clauset, "Detecting change points in the large-scale structure of evolving networks," in *Proceedings of the AAAI Conference on Artificial Intelligence*, vol. 29, no. 1, 2015.

[46] S. Roy, Y. Atchadé, and G. Michailidis, "Change point estimation in high dimensional Markov random-field models," *Journal of the Royal Statistical Society. Series B, Statistical methodology*, vol. 79, no. 4, p. 1187, 2017.

[47] X. Jiang, S. Mahadevan, and A. Urbina, "Bayesian nonlinear structural equation modeling for hierarchical validation of dynamical systems," *Mechanical Systems and Signal Processing*, vol. 24, no. 4, pp. 957–975, 2010.

[48] J. R. Harring, B. A. Weiss, and J.-C. Hsu, "A comparison of methods for estimating quadratic effects in nonlinear structural equation models," *Psychological Methods*, vol. 17, no. 2, p. 193, 2012.

[49] Y. Shen, B. Baingana, and G. B. Giannakis, "Kernel-based structural equation models for topology identification of directed networks," *IEEE Transactions on Signal Processing*, vol. 65, no. 10, pp. 2503–2516, 2017.

[50] A. H. Sayed *et al.*, "Adaptation, learning, and optimization over networks," *Foundations and Trends® in Machine Learning*, vol. 7, no. 4-5, pp. 311–801, 2014.

[51] K. R. Davidson and S. J. Szarek, "Local operator theory, random matrices and banach spaces," *Handbook of the geometry of Banach spaces*, vol. 1, no. 317-366, p. 131, 2001.

[52] T. Sarkar and A. Rakhlin, "Near optimal finite time identification of arbitrary linear dynamical systems," in *International Conference on Machine Learning*. PMLR, 2019, pp. 5610–5618.

[53] R. O. Saber and R. M. Murray, "Consensus protocols for networks of dynamic agents," in *2003 American Control Conference*, vol. 2. IEEE, 2003, pp. 951–956.

[54] L. Moreau, "Stability of multiagent systems with time-dependent communication links," *IEEE Transactions on Automatic Control*, vol. 50, no. 2, pp. 169–182, 2005.

Yushan Li (S'19) received the B.E. degree in School of Artificial Intelligence and Automation from Huazhong University of Science and Technology, Wuhan, China, in 2018. He is currently working toward the Ph.D. degree with the Department of Automation, Shanghai Jiaotong University, Shanghai, China. He is a member of Intelligent of Wireless Networking and Cooperative Control group. His research interests include robotics, security of cyber-physical system, and distributed computation and optimization in multi-agent networks.

Jianping He (SM'19) is currently an associate professor in the Department of Automation at Shanghai Jiao Tong University. He received the Ph.D. degree in control science and engineering from Zhejiang University, Hangzhou, China, in 2013, and had been a research fellow in the Department of Electrical and Computer Engineering at University of Victoria, Canada, from Dec. 2013 to Mar. 2017. His research interests mainly include the distributed learning, control and optimization, security and privacy in network systems.

Dr. He serves as an Associate Editor for IEEE Open Journal of Vehicular Technology and KSII Trans. Internet and Information Systems. He was also a Guest Editor of IEEE TAC, International Journal of Robust and Nonlinear Control, etc. He was the winner of Outstanding Thesis Award, Chinese Association of Automation, 2015. He received the best paper award from IEEE WCSP'17, the best conference paper award from IEEE PESGM'17, and was a finalist for the best student paper award from IEEE ICCA'17.

Cailian Chen (M'06) received the B.E. and M.E. degrees in Automatic Control from Yanshan University, P. R. China in 2000 and 2002, respectively, and the Ph.D. degree in Control and Systems from City University of Hong Kong, Hong Kong SAR in 2006. She joined Department of Automation, Shanghai Jiao Tong University in 2008 as an Associate Professor. She is now a Full Professor. Before that, she was a postdoctoral research associate in University of Manchester, U.K. (2006–2008). She was a Visiting Professor in University of Waterloo, Canada (2013–2014). Prof. Chen's research interests include industrial wireless networks, computational intelligence and situation awareness, Internet of Vehicles.

Prof. Chen has authored 3 research monographs and over 100 referred international journal papers. She is the inventor of more than 20 patents. She received the prestigious "IEEE Transactions on Fuzzy Systems Outstanding Paper Award" in 2008, and Best Paper Award of WCSP17 and YAC18. She won the Second Prize of National Natural Science Award from the State Council of China in 2018, First Prize of Natural Science Award from The Ministry of Education of China in 2006 and 2016, respectively, and First Prize of Technological Invention of Shanghai Municipal, China in 2017. She was honored Changjiang Young Scholar in 2015 and Excellent Young Researcher by NSF of China in 2016. Prof. Chen has been actively involved in various professional services. She serves as Associate Editor of IEEE Transactions on Vehicular Technology, Peer-to-peer Networking and Applications (Springer). She also served as Guest Editor of IEEE Transactions on Vehicular Technology, TPC Chair of ISAS19, Symposium TPC Co-chair of IEEE Globecom 2016 and VTC2016-fall, Workshop Co-chair of WiOpt18.

Xinping Guan (F'18) received the B.S. degree in Mathematics from Harbin Normal University, Harbin, China, in 1986, and the Ph.D. degree in Control Science and Engineering from Harbin Institute of Technology, Harbin, China, in 1999. He is currently a Chair Professor with Shanghai Jiao Tong University, Shanghai, China, where he is the Dean of School of Electronic, Information and Electrical Engineering, and the Director of the Key Laboratory of Systems Control and Information Processing, Ministry of Education of China. Before that, he was the Professor and Dean of Electrical Engineering, Yanshan University, Qinhuangdao, China.

Dr. Guan's current research interests include industrial cyber-physical systems, wireless networking and applications in smart factory, and underwater networks. He has authored and/or coauthored 5 research monographs, more than 270 papers in IEEE Transactions and other peer-reviewed journals, and numerous conference papers. As a Principal Investigator, he has finished/been working on many national key projects. He is the leader of the prestigious Innovative Research Team of the National Natural Science Foundation of China (NSFC). Dr. Guan is an Executive Committee Member of Chinese Automation Association Council and the Chinese Artificial Intelligence Association Council. Dr. Guan received the First Prize of Natural Science Award from the Ministry of Education of China in both 2006 and 2016, and the Second Prize of the National Natural Science Award of China in both 2008 and 2018. He was a recipient of IEEE Transactions on Fuzzy Systems Outstanding Paper Award in 2008. He is a National Outstanding Youth honored by NSF of China, Changjiang Scholar by the Ministry of Education of China and State-level Scholar of New Century Bai Qianwan Talent Program of China.